Please cite this article in press as: Zafra-Puerta et al., Gene therapy for Lafora disease in the *Epm2a*$^{-/-}$ mouse model, Molecular Therapy (2024), https://doi.org/10.1016/j.ymthe.2024.05.032

Molecular Therapy
Original Article

Gene therapy for Lafora disease in the *Epm2a*$^{-/-}$ mouse model

Luis Zafra-Puerta,[1,2,3,5] Nerea Iglesias-Cabeza,[1,2] Daniel F. Burgos,[1,2,3] Miriam Sciaccaluga,[4,5] Juan González-Fernández,[1,2,6] Laura Bellingacci,[7] Jacopo Canonichesi,[4] Gema Sánchez-Martín,[1,2] Cinzia Costa,[4] Marina P. Sánchez,[1,2] and José M. Serratosa[1,2]

[1]Laboratory of Neurology, Instituto de Investigación Sanitaria-Fundación Jiménez Díaz, Universidad Autónoma de Madrid (IIS-FJD, UAM), 28040 Madrid, Spain; [2]Centro de Investigación Biomédica en Red de Enfermedades Raras (CIBERER), 28029 Madrid, Spain; [3]PhD Program in Neuroscience, Universidad Autonoma de Madrid-Cajal Institute, 28029 Madrid, Spain; [4]Section of Neurology, Department of Medicine and Surgery, University of Perugia, 06132 Perugia, Italy; [5]Fondazione Malattie Rare Mauro Baschirotto BIRD Onlus, Longare (VI), Italy; [6]Departament of Microbiology and Parasitology, Faculty of Pharmacy, Complutense University of Madrid, University of Perugia, 06132 Perugia, Italy; [7]Section of Physiology and Biochemistry, Department of Medicine and Surgery, University of Perugia, 06132 Perugia, Italy

Lafora disease is a rare and fatal form of progressive myoclonic epilepsy typically occurring early in adolescence. The disease results from mutations in the *EPM2A* gene, encoding laforin, or the *EPM2B* gene, encoding malin. Laforin and malin work together in a complex to control glycogen synthesis and prevent the toxicity produced by misfolded proteins via the ubiquitin-proteasome system. Disruptions in either protein cause alterations in this complex, leading to the formation of Lafora bodies containing abnormal, insoluble, and hyperphosphorylated forms of glycogen. We used the *Epm2a*$^{-/-}$ knockout mouse model of Lafora disease to apply gene therapy by administering intracerebroventricular injections of a recombinant adeno-associated virus carrying the human *EPM2A* gene. We evaluated the effects of this treatment through neuropathological studies, behavioral tests, video-electroencephalography, electrophysiological recordings, and proteomic/phosphoproteomic analysis. Gene therapy ameliorated neurological and histopathological alterations, reduced epileptic activity and neuronal hyperexcitability, and decreased the formation of Lafora bodies. Moreover, differential quantitative proteomics and phosphoproteomics revealed beneficial changes in various molecular pathways altered in Lafora disease. Our results represent proof of principle for gene therapy with the coding region of the human *EPM2A* gene as a treatment for *EPM2A*-related Lafora disease.

INTRODUCTION

Lafora disease (OMIM: 254780. ORPHA: 501) is a rare and fatal form of neurodegenerative disease that appears in early adolescence with seizures and a progressive neurological decline with dementia resulting in death within 5–15 years.[1–3] Unfortunately, there is no specific therapy, and patients can only receive antiseizure medications to temporarily manage seizures.[4] The disease is caused by autosomal recessive inherited mutations in either the *EPM2A* (OMIM: 607566) gene, encoding the dual-specificity phosphatase laforin,[5–8] or the *EPM2B* (OMIM: 608072) gene, encoding the E3-ubiquitin ligase malin.[9,10] Laforin is a glucan phosphatase acting as an adapter protein of enzymes involved in glycogen synthesis, an adapter protein in endoplasmic reticulum (ER) stress and protein clearance, and a tumor suppressor protein.[11] The laforin-malin complex regulates glycogen metabolism by inducing proteasome-dependent degradation of muscle glycogen synthase (GS), glycogen debranching enzyme (GDE), and protein targeting to glycogen (PTG).[11,12] Additionally, the laforin-malin complex helps mitigate the toxicity produced by misfolded proteins through the ubiquitin-proteasome system (UPS).[13] Disruptions in laforin or malin lead to the formation of aggregates of abnormal, insoluble, poorly branched, and hyperphosphorylated forms of glycogen, known as Lafora bodies (LBs).[14–17] Alterations in oxidative stress, protein misfolding, and proteasomal dysfunction also contribute to the pathophysiology of the disease.[18–20]

Different murine models of Lafora disease have been generated, including the *Epm2a*$^{-/-}$ and *Epm2b*$^{-/-}$ knockout mice.[21,22] These models replicate, although with a milder phenotype, most of the neurological alterations seen in patients, such as neuroinflammation, neurodegeneration, LB formation, neuronal hyperexcitability, cognitive deficits, and motor impairment.[23] *Epm2a*$^{-/-}$ and *Epm2b*$^{-/-}$ knockout mouse models have been used to assay different putative treatments to cure or ameliorate the symptoms of the disease. Thus, we showed in these models that metformin improved many neurological alterations.[24,25] Subsequently, we showed that, in early-stage patients, metformin slows the progression of symptoms and the decline in the performance of activities of daily living[24] compared to treatments in patients in more advanced stages of the disease.[26]

Received 22 December 2023; accepted 23 May 2024;
https://doi.org/10.1016/j.ymthe.2024.05.032.

Correspondence: Marina P. Sánchez, Laboratory of Neurology, Instituto de Investigación Sanitaria-Fundación Jiménez Díaz, Universidad Autónoma de Madrid (IIS-FJD, UAM), 28040 Madrid, Spain.
E-mail: msanchezg@fjd.es
Correspondence: José M. Serratosa, Laboratory of Neurology, Instituto de Investigación Sanitaria-Fundación Jiménez Díaz, Universidad Autónoma de Madrid (IIS-FJD, UAM), 28040 Madrid, Spain.
E-mail: joseserratosa@me.com

All rights are reserved, including those for text and data mining, AI training, and similar technologies.

Please cite this article in press as: Zafra-Puerta et al., Gene therapy for Lafora disease in the *Epm2a*$^{-/-}$ mouse model, Molecular Therapy (2024), https://doi.org/10.1016/j.ymthe.2024.05.032

Alternative therapeutic strategies, such as sodium selenate,[27] VAL-0417,[28] the antisense oligonucleotide Gys1-ASO that targets the mRNA of the brain-expressed GS 1,[29] and various modulators of neuroinflammation, have also been assessed in animal models.[30] Down-regulation of the *Gys1* gene through AAV9-delivered Gys1-directed CRISPR-Cas9[31] or microRNA (miRNA)[32] also resulted in a remarkable reduction in polyglucosan body formation and a slight reduction of neuroinflammatory markers.

Recombinant adeno-associated viruses (rAAVs) are widely used vectors for gene therapy. They are non-pathogenic, produce low immunological responses, rarely integrate into the host genome, have a broad tropism, and allow long-term transgene expression. These viruses are small, non-enveloped, single-stranded (ss) DNA particles belonging to the Parvoviridae family, genus Dependoviridae. To date, more than 10 different adeno-associated virus (AAV) serotypes and more than 100 variants have been isolated from adenovirus stocks and human/non-human primate tissues. Different serotypes have different tropisms and recent progress in the field has led to precise targeting toward specific tissues of interest.[33–41]

Here, we show that the rAAV2/9-CAG-h*EPM2A* (rAAV-h*EPM2A*) vector, containing the coding region of the human *EPM2A* (h*EPM2A*) gene, significantly diminishes neurological and histopathological alterations, reduces epileptic activity, and rescues electrophysiological deficits in the *Epm2a*$^{-/-}$ mouse model of Lafora disease. We also show, through differential quantitative proteomic and phosphoproteomic analysis, that human laforin produces beneficial changes in certain molecular pathways altered in Lafora disease. This molecular analysis is crucial for comprehending gene therapy mechanisms of action and understanding specific processes that are corrected by replacing *EPM2A*.

RESULTS

The rAAV-h*EPM2A* vector efficiently transduces central nervous system cells in *Epm2a*$^{-/-}$ mice, leading to transcription and translation of the h*EPM2A* transgene

Three months after a single intracerebroventricular (i.c.v.) injection of rAAV-*GFP* or rAAV-h*EPM2A* in 3-month-old *Epm2a*$^{-/-}$ mice, we verified the successful transduction of the vectors in central nervous system (CNS) cells. First, we confirmed h*EPM2A* transgene transcription through RT-PCR (Figure S1A). Next, using an antibody against GFP, we observed expression of the *GFP* transgene in the hippocampus, cortex, septal nuclei, and fimbria (Figure S1B).

Transcription of the h*EPM2A* transgene was quantified by RT-qPCR in RNA samples from the total brain of *Epm2a*$^{-/-}$ mice 3 and 9 months after a single i.c.v. injection of rAAV-h*EPM2A* vector (Figures S2A and S2B). Gene expression levels were similar to those of endogenous *Epm2a* in wild-type (WT) animals and did not change over time, although we did observe inter-animal variability (Figures S2A and S2B). Additionally, RNA translation was analyzed with an antibody against laforin, demonstrating effective protein expression in the hippocampus, cortex, the region of the fornix and the septofimbrial and lateral septal nuclei, both 3 and 9 months after rAAV-h*EPM2A* injection, without showing differences in expression over time (Figure S2C). To identify the cell type where laforin was expressed, the colocalization of laforin and neuronal nuclei (NeuNs), and laforin and glial fibrillary acidic protein (GFAP), was assessed (Figures 1 and S3). Laforin preferentially labeled NeuN-positive pyramidal neurons of cortical layer V and the CA1 and CA2–CA3 fields of the hippocampus (Figures 1A and S3A). A slight level of laforin expression was also found in GFAP-positive cells in the same regions (Figures 1B and S3B).

i.c.v. injection of rAAV-h*EPM2A* prevents LB formation in the brain of *Epm2a*$^{-/-}$ mice

We analyzed and quantified the number of LBs in the CA1 (Figures 2A and 2C) and CA2–CA3 (Figures 2B and 2D) regions of the hippocampus and in layers IV–V of the sensorimotor cortex (Figures 2E and 2F) 3 and 9 months after injections of rAAV-h*EPM2A* and rAAV-Null. We also analyzed the progression of LB formation at baseline and 3 and 9 months after i.c.v. injections (Figure 2G). Treated mice showed a significant decrease in the number of LBs in the CA1 and CA2–CA3 regions of the hippocampus (Figures 2C and 2D) 9 months after treatment administration, as well as a slower progression of the formation of these aberrant molecules compared to animals injected with rAAV-Null (Figure 2G). When analyzing the number of LBs in layers IV–V of the sensorimotor cortex (magnified box in Figure 2E), we did not observe significant differences between treated and control animals (Figure 2F); however, we found that the progression of LB formation was slower in mice treated with rAAV-h*EPM2A* (Figure 2G).

Treatment with rAAV-h*EPM2A* in *Epm2a*$^{-/-}$ mice decreases astrogliosis, microgliosis, and cell death

The effect of rAAV-h*EPM2A* on neuroinflammation in *Epm2a*$^{-/-}$ mice was assessed 3 and 9 months after i.c.v. injections using GFAP (Figures 3 and S4A–S4C) and Iba1 (Figures S4D–S4F) antibodies to stain sections from different regions of the hippocampus and cerebral cortex. We analyzed the CA1 field with GFAP and observed a reduction in reactive astrocytes 3 and 9 months after injection (Figures 3A–3C). In the sensorimotor cortex, a decrease in the number of GFAP-positive cells was also found 3 months post rAAV-h*EPM2A* injection, although 9 months later the results were not statistically significant (Figures 3D–3F). We observed a significant decrease in the number of reactive astrocytes in the CA2–CA3 region of the hippocampus 3 months after rAAV-h*EPM2A* injection in *Epm2a*$^{-/-}$ mice (Figures S4A and S4B). Although there was a trend toward decrease in the number of reactive astrocytes 9 months after injection, the results did not reach statistical significance (Figures S4A and S4C). When analyzing microglia with the Iba-1 antibody in the CA2–CA3 fields of the hippocampus of *Epm2a*$^{-/-}$ mice injected with the rAAV-Null vector, we found a significantly higher number of Iba-1-positive cells compared to WT mice 9 months after injection (Figures S4D and S4F). Treatment with rAAV-h*EPM2A* normalized

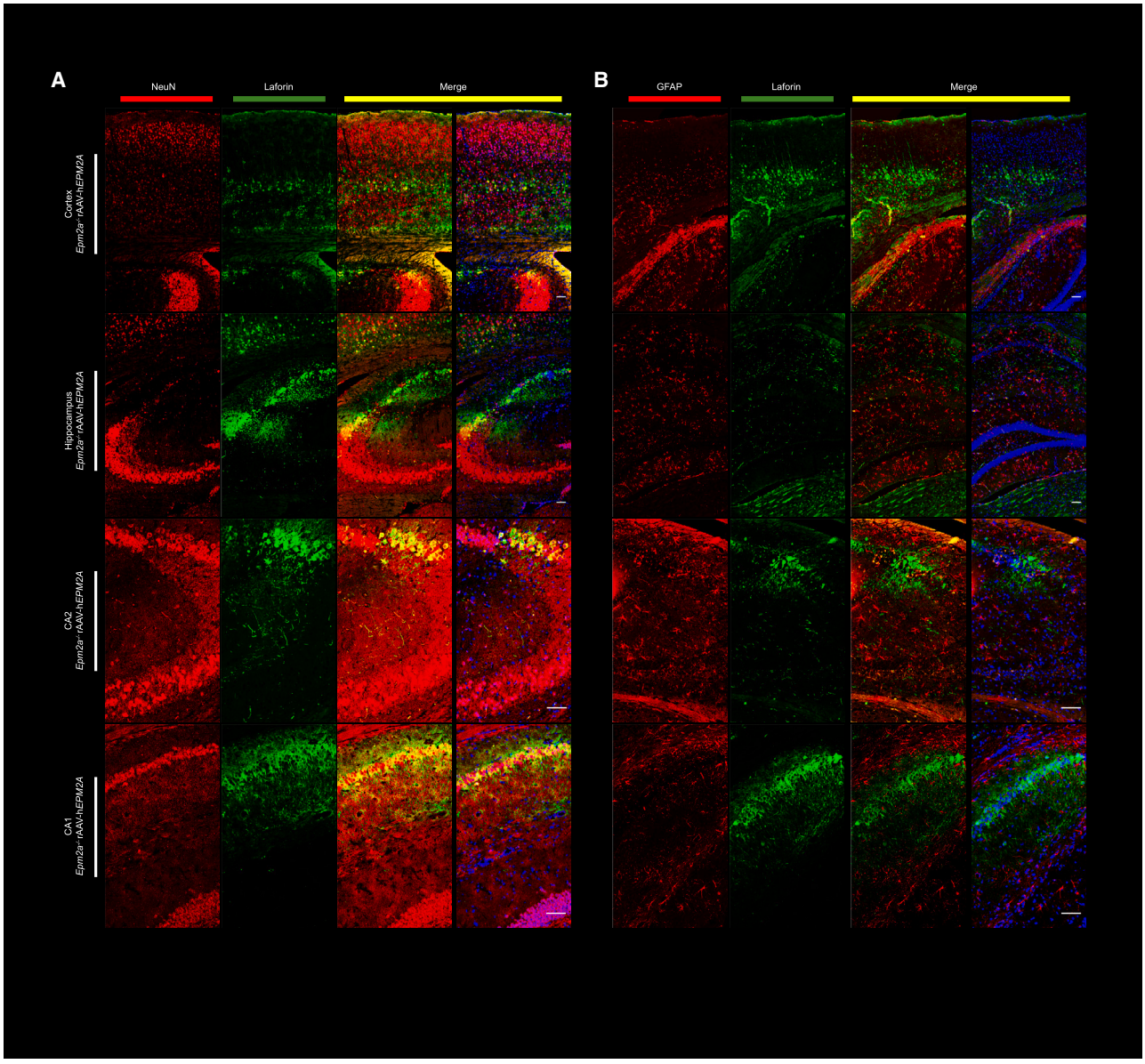

Figure 1. Expression of the transgene in neurons and astrocytes

(A) Double IF-P staining was performed to identify cells expressing laforin (green) and NeuN (red), confirming that laforin is correctly expressed in neurons (yellow) of the deep layers of the cortex and in those of the CA1 and CA2 regions of the hippocampus, following i.c.v. injection of rAAV-h*EPM2A*. (B) Similarly, laforin (green) and GFAP (red) immunostaining showed that laforin is expressed in astrocytes (yellow) of the cortex and hippocampus, although at lower levels compared to neuronal transduction. Scale bar, 50 μm. See also Figure S3.

the number of microglial cells in *Epm2a*$^{-/-}$ mice compared to WT mice (Figures S4D and S4F).

The effect of rAAV-h*EPM2A* on neurodegeneration was examined using the NeuN antibody to analyze different regions of the hippocampus and the sensorimotor cortex (Figures S6 and S7). A tendency toward reducing neuronal loss in the CA1 region was observed in *Epm2a*$^{-/-}$ mice 3 months after the treatment administration; however, no statistically significant changes in neurodegeneration were observed in any brain region (Figures S6A–S6C and S7).

Given the clear tendency to recover neuronal loss in *Epm2a*$^{-/-}$ mice treated with rAAV-h*EPM2A* at 3 months post injection, we analyzed the levels of cleaved caspase-3 in the CA1 and CA2–CA3 regions of the hippocampus and in the layers IV–V of the sensorimotor cortex. We observed a significant decrease in cleaved caspase 3-positive cells

Please cite this article in press as: Zafra-Puerta et al., Gene therapy for Lafora disease in the *Epm2a*$^{-/-}$ mouse model, Molecular Therapy (2024), https://doi.org/10.1016/j.ymthe.2024.05.032

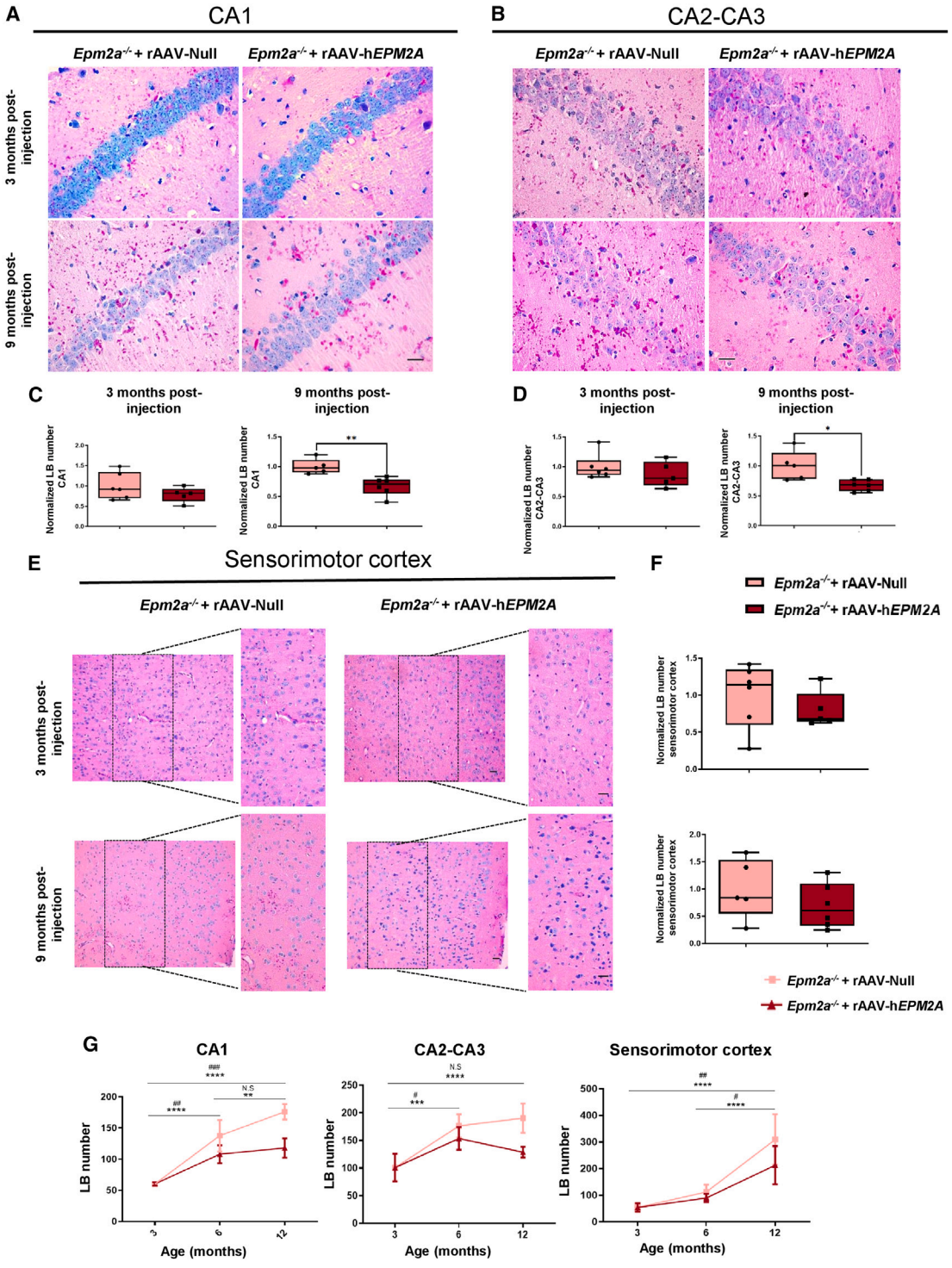

Figure 2. Quantification of LB formation in the CA1 and CA2–CA3 regions of the hippocampus and in layers IV and V of the sensorimotor cortex of *Epm2a*$^{-/-}$ mice treated with rAAV-h*EPM2A*

(A, B, and E) Periodic acid–Schiff (PAS)-Diastase (PAS-D) staining in the CA1 (A) and CA2–CA3 (B) regions of the hippocampus and in layers IV and V of the sensorimotor cortex (E) of *Epm2a*$^{-/-}$ mice 3 and 9 months after i.c.v. administration of rAAV-h*EPM2A* or rAAV-Null. (C, D, and F) Quantitative comparison of LB number in the different regions. In the sensorimotor cortex, it the region zoomed in was quantified (width, 747 px; height, 1,550 px), corresponding to layers IV and V. Results are expressed as the

(legend continued on next page)

in the CA1 and CA2–CA3 fields of the hippocampus of treated mice (Figure S5), but not in the sensorimotor cortex (data not shown). These data suggest that treatment with rAAV-h*EPM2A* reduces cell death in the hippocampus.

Gene therapy with rAAV-h*EPM2A* i.c.v. injection in *Epm2a*$^{-/-}$ mice delays the onset of memory decline and diminishes motor impairments

We analyzed the effects of laforin expression on episodic memory, motor coordination, and spontaneous locomotor activity. Memory performance was significantly improved in *Epm2a*$^{-/-}$-treated mice 3 months after injection, as indicated by their higher discrimination index (Figure 4A). This effect, however, was not seen in *Epm2a*$^{-/-}$-treated mice 9 months post injection (Figure 4B) since memory failures were absent at this time even in control *Epm2a*$^{-/-}$ mice (injected with rAAV-Null).

Motor coordination was also improved with treatment, as shown by increased latency to fall from the rod on the rotarod 3 and 9 months post injection (Figures 4C and 4D). Three months after i.c.v. injection, *Epm2a*$^{-/-}$ control mice (*Epm2a*$^{-/-}$ + rAAV-Null) showed a significantly shorter cylinder drop latency time in the rotarod test than the healthy WT control (Figure 4C), showing the alterations in motor coordination present in the model. However, the *Epm2a*$^{-/-}$ mice that received the treatment lasted longer in the cylinder than the *Epm2a*$^{-/-}$ mice injected with rAAV-Null and experienced no significant differences compared to the WT injected with rAAV-Null (Figure 4C). Nine months after the i.c.v. injection, this difference became more noticeable, completely normalizing the cylinder drop latency times between treated *Epm2a*$^{-/-}$ and WT mice (Figure 4D).

Analysis of spontaneous motor activity in the actimeter revealed improved performance of *Epm2a*$^{-/-}$-treated mice 3 months after injection. However, the treatment resulted in a greater spontaneous motor activity compared to WT mice, denoting certain hyperactivity (Figure 4E). Nine months after treatment with rAAV-h*EPM2A*, *Epm2a*$^{-/-}$ mice did not exhibit an increased spontaneous locomotor activity compared to *Epm2a*$^{-/-}$ injected with rAAV-Null, although treated mice presented a partially reduced hyperactivity (Figure 4F).

Treatment with rAAV-h*EPM2A* in *Epm2a*$^{-/-}$ mice reduces EEG power, frequency of interictal epileptiform discharges, and their heightened sensitivity to pentylenetetrazole

Video-electroencephalography (EEG) recordings were performed in 12-month-old mice (9 months after injection) to examine epileptic-like activity. *Epm2a*$^{-/-}$-treated mice exhibited normalized basal activity rhythms, showing lower beta and gamma wave power spectra compared to *Epm2a*$^{-/-}$ mice injected with rAAV-Null (Figure 5A). Following the administration of a subconvulsive dose of pentylenetetrazole (PTZ) (30 mg/kg), power spectra decreased in all groups. However, the decrease was more significant in *Epm2a*$^{-/-}$ mice injected with rAAV-Null compared to WT or *Epm2a*$^{-/-}$-treated mice (Figure 5B). Furthermore, analysis of spontaneous (Figure 5C) and 30-mg/kg PTZ-induced (Figure 5D) interictal epileptiform discharges (IEDs) indicated that *Epm2a*$^{-/-}$-treated mice experienced fewer spontaneous IEDs than those injected with rAAV-Null (Figure 5C).

Additionally, *Epm2a*$^{-/-}$-treated mice displayed a reduced incidence of myoclonic jerks in response to intraperitoneal (i.p.) injection of PTZ (30 mg/kg), compared to *Epm2a*$^{-/-}$ mice injected with rAAV-Null, 3 months after injection (Figure 5E). We found that treatment produced a tendency toward fewer myoclonic jerks 9 months post injection (Epm2a mice with myoclonic jerks: 60% *Epm2a*$^{-/-}$ +rAAV-Null vs. 33.3% *Epm2a*$^{-/-}$ + rAAV-hEPM2A) (Figure 5F), although differences were not statistically significant. Nine months after an i.p. injection of PTZ (50 mg/kg), *Epm2a*$^{-/-}$-treated mice exhibited a significant lower mortality (Figure 5H) and fewer generalized tonic-clonic (GTC) seizures (Figure 5G).

The rAAV-h*EPM2A* vector restores physiological firing properties in the CA1 region of *Epm2a*$^{-/-}$ mice

Electrophysiological characterization of the hippocampal circuit of *Epm2a*$^{-/-}$ mice showed unaltered membrane properties of CA1 pyramidal neurons. Indeed, membrane capacitance, voltage-current relationship, and resting membrane potential, albeit with a trend toward greater depolarization for *Epm2a*$^{-/-}$ cells, showed no significant differences between experimental groups (Figures S8A and S8B). As shown in the histograms, gene therapy treatment did not alter the physiological membrane properties of pyramidal neurons. In contrast, the analysis of the number of action potentials (APs) evoked by the injection of depolarizing steps of current showed a significant

median of independent samples. The bars in the box plots show the minimum and maximum values. Values were normalized using values from *Epm2a*$^{-/-}$ mice injected with rAAV-Null. A non-parametric Mann-Whitney test was performed. Nine months after injection, CA1 region, *Epm2a*$^{-/-}$ + rAAV-Null vs. *Epm2a*$^{-/-}$ + rAAV-h*EPM2A* $p = 0.0043$; 9 months after injection, CA2–CA3 region, *Epm2a*$^{-/-}$ + rAAV-Null vs. *Epm2a*$^{-/-}$ + rAAV-h*EPM2A* $p = 0.0173$). (G) Comparative progression of LB formation over time in different brain regions of *Epm2a*$^{-/-}$ mice treated with rAAV-h*EPM2A* or injected with rAAV-Null. A two-way ANOVA with Tukey's multiple comparisons test was performed. Data are shown as mean (SD). Asterisks (*) indicate differences in the progression of LB formation over time in *Epm2a*$^{-/-}$ mice injected with rAAV-Null; hash symbols (#) indicate differences in the progression of LB formation over time in *Epm2a*$^{-/-}$ mice treated with rAAV-h*EPM2A*. CA1region: *Epm2a*$^{-/-}$ mice injected with rAAV-Null from 3 to 6 months, $p = <.001$; *Epm2a*$^{-/-}$ mice injected with rAAV-Null from 3 to 12 months, $p = <.001$; *Epm2a*$^{-/-}$ mice injected with rAAV-Null from 6 to 12 months, $p = 0.0067$; *Epm2a*$^{-/-}$ mice treated with rAAV- h*EPM2A* from 3 to 6 months, $p = 0.0019$; *Epm2a*$^{-/-}$ mice treated with rAAV- h*EPM2A* from 3 to 12 months $p = <.001$. CA2–CA3 region: *Epm2a*$^{-/-}$ mice injected with rAAV-Null from 3 to 6 months, $p = <.001$; *Epm2a*$^{-/-}$ mice injected with rAAV-Null from 3 to 12 months, $p = <.001$; *Epm2a*$^{-/-}$ mice treated with rAAV- h*EPM2A* from 3 to 6 months, $p = 0.0175$. Layers IV-V of the sensorimotor cortex: *Epm2a*$^{-/-}$ mice injected with rAAV-Null from 3 to 12 months, $p = <.001$; *Epm2a*$^{-/-}$ mice injected with rAAV-Null from 6 to 12 months, $p = <.001$; *Epm2a*$^{-/-}$ mice treated with rAAV- h*EPM2A* from 3 to 12 months, $p = 0.0017$; *Epm2a*$^{-/-}$ mice treated with rAAV- h*EPM2A* from 6 to 12 months, $p = 0.0129$. $^{*}p < 0.05$, $^{**}p < 0.01$, $^{***}p < 0.001$, $^{****}p < 0.0001$; N.S., not significant. $n = 4$–6 mice per group. Scale bar, 25 μm (A and B) and 50 μm (E).

Please cite this article in press as: Zafra-Puerta et al., Gene therapy for Lafora disease in the *Epm2a*$^{-/-}$ mouse model, Molecular Therapy (2024), https://doi.org/10.1016/j.ymthe.2024.05.032

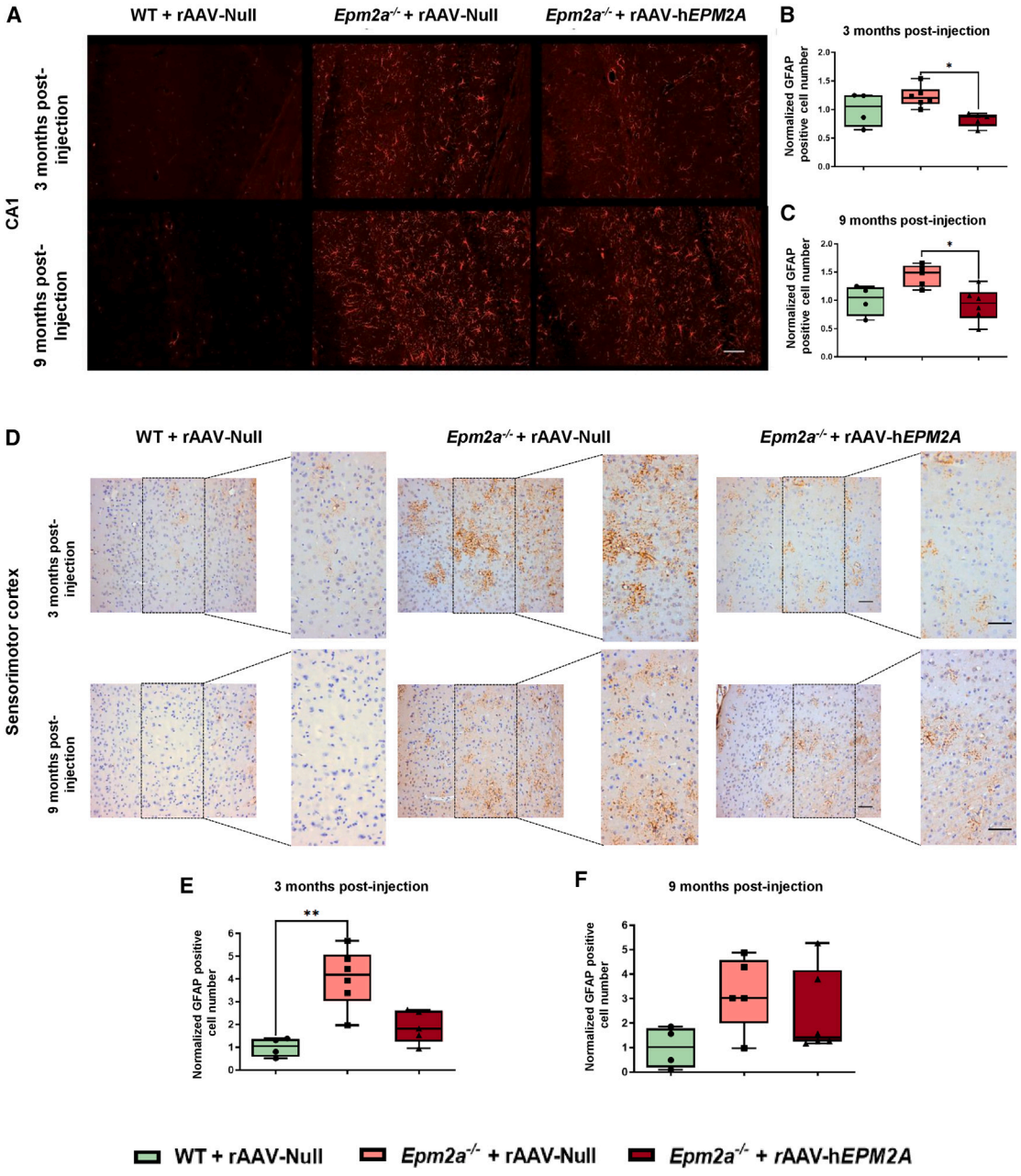

Figure 3. Astrogliosis in the CA1 region of the hippocampus and in layers IV and V of the sensorimotor cortex in *Epm2a*$^{-/-}$ mice

(A and D) IHC with anti-GFAP antibody in the CA1 region of the hippocampus (A) and in layers IV and V of the sensorimotor cortex (D) of WT mice injected with rAAV-Null and *Epm2a*$^{-/-}$ mice treated with rAAV-h*EPM2A* or injected with rAAV-Null 3 and 9 months after i.c.v. injection. (B and C) Quantification of reactive astrocytes in the CA1 region of the hippocampus of WT mice injected with rAAV-Null and *Epm2a*$^{-/-}$ mice treated with rAAV-h*EPM2A* or injected with rAAV-Null 3 months (*Epm2a*$^{-/-}$ + rAAV-Null vs. *Epm2a*$^{-/-}$ + rAAV-h*EPM2A*, $p = 0.0374$) (B) and 9 months (*Epm2a*$^{-/-}$ + rAAV-Null vs. *Epm2a*$^{-/-}$ + rAAV-h*EPM2A* $p = 0.0325$) (C) after injection. (E and F) Quantification of reactive astrocytes in layers IV and V of the sensorimotor cortex in WT mice injected with rAAV-Null and *Epm2a*$^{-/-}$ mice treated with rAAV-h*EPM2A* or injected with rAAV-Null 3 months (WT + rAAV-Null vs. *Epm2a*$^{-/-}$ + rAAV-Null $p = 0.0045$) (E) and 9 months (F) after injection. The quantification was carried out in the region zoomed in (width, 747 px; height, 1550 px), corresponding to layers IV and V. Results are expressed as the median of independent samples. The bars in the box plots show the minimum and maximum values. Values were normalized using the values of WT mice injected with rAAV-Null. A non-parametric Kruskal-Wallis test followed by Dunn's multiple comparisons test was performed. $^{*}p < 0.05$, $^{**}p < 0.01$. $n = 4$–6 mice per group. Scale bar, 50 μm.

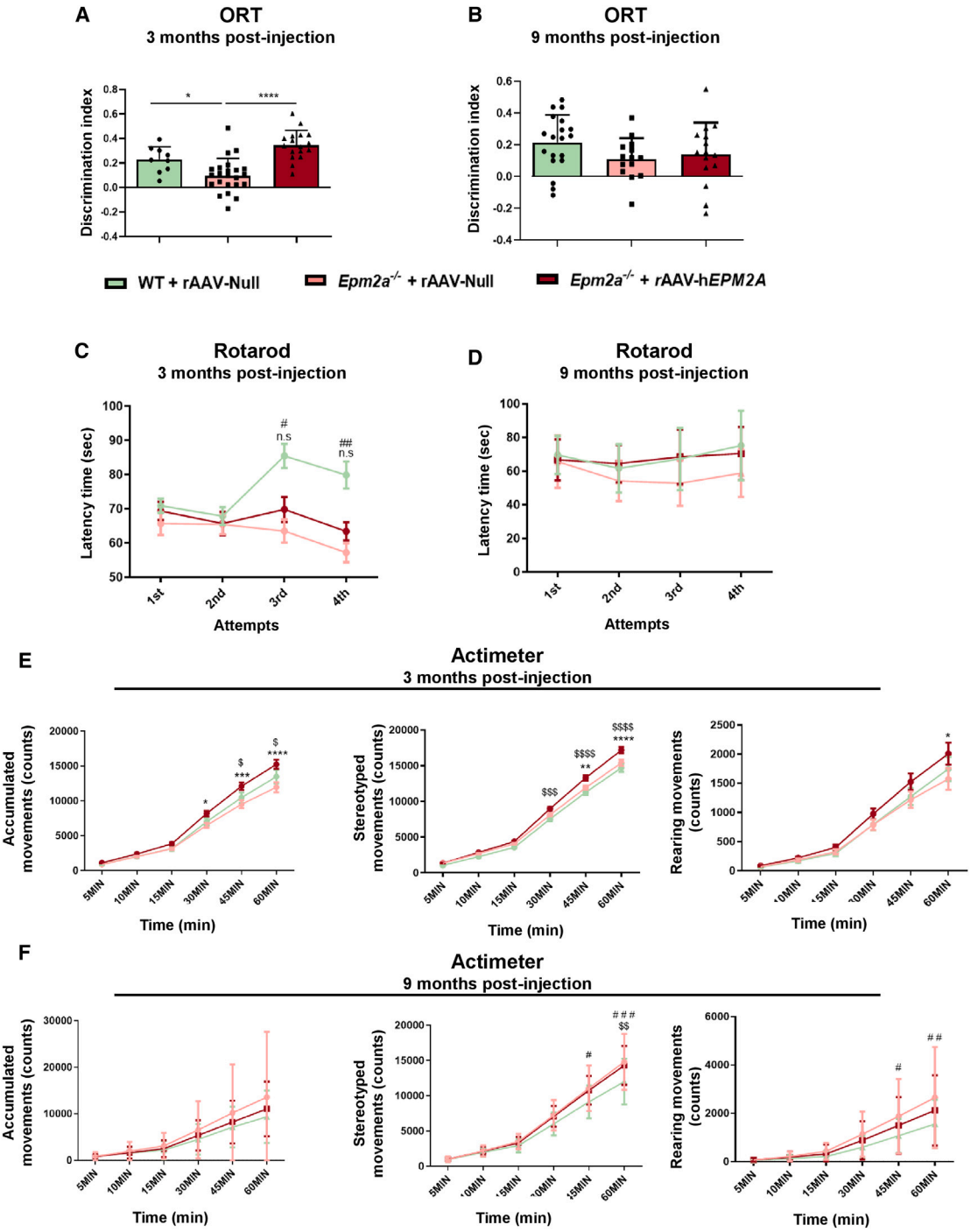

Figure 4. Behavioral studies in *Epm2a*$^{-/-}$ mice treated with rAAV-h*EPM2A* or rAAV-Null 3 and 9 months after injection

(A and B) Memory assessment based on DI evaluation in the ORT, 3 months (WT vs. *Epm2a*$^{-/-}$ + rAAV-Null, $p = 0.0332$; *Epm2a*$^{-/-}$ + rAAV-h*EPM2A* vs. *Epm2a*$^{-/-}$ + rAAV-Null, $p < 0.001$) (A) and 9 months (B) after injection. (C and D) Evaluation of motor coordination based on the latency time to fall from the cylinder of *Epm2a*$^{-/-}$ mice 3 months (WT vs. *Epm2a*$^{-/-}$ + rAAV-Null third attempt, $p = 0.0102$; WT vs. *Epm2a*$^{-/-}$ + rAAV-Null fourth attempt, $p = 0.0083$; no significant differences were found in WT vs. *Epm2a*$^{-/-}$ + rAAV-h*EPM2A*) 3 months (C) and 9 months (D) after injection. (E and F) Analysis of spontaneous accumulated, stereotyped, and rearing movements of *Epm2a*$^{-/-}$ mice 3 months after injection (E) (accumulated movement counts: *Epm2a*$^{-/-}$ + rAAV-h*EPM2A* vs. *Epm2a*$^{-/-}$ + rAAV-Null 30′, $p = 0.0417$, 45′ and 60′, $p < 0.001$; *Epm2a*$^{-/-}$ + rAAV-h*EPM2A* vs. WT + rAAV-Null 45′, $p = 0.0414$; *Epm2a*$^{-/-}$ + rAAV-h*EPM2A* vs. WT + rAAV-Null 60′, $p = 0.0239$. Stereotyped movement counts: *Epm2a*$^{-/-}$ + rAAV-h*EPM2A* vs. *Epm2a*$^{-/-}$ + rAAV-Null 45′, $p = 0.0019$, 60′, $p < 0.001$; *Epm2a*$^{-/-}$ + rAAV-h*EPM2A* vs. WT + rAAV-Null 30′, 45′ and 60′, $p < 0.001$. Rearing movement counts: *Epm2a*$^{-/-}$ + rAAV-h*EPM2A* vs.

(legend continued on next page)

Please cite this article in press as: Zafra-Puerta et al., Gene therapy for Lafora disease in the *Epm2a*$^{-/-}$ mouse model, Molecular Therapy (2024), https://doi.org/10.1016/j.ymthe.2024.05.032

increase in the number of APs in the first step (50 pA) of injected current. This demonstrates an initial intrinsic hyperexcitability; however, this is not maintained due to a probable failure of the repolarization mechanisms of CA1 pyramidal neurons in *Epm2a*$^{-/-}$ animals injected with rAAV-Null (Figure 6A). In parallel, we found a trend toward reduced rheobase current and a significant depolarized threshold potential in *Epm2a*$^{-/-}$ animals injected with rAAV-Null (Figure 6B). Treatment with the rAAV-h*EPM2A* vector completely restored the firing properties of CA1 pyramidal neurons and the threshold potential 3 months after injection (Figures 6A and 6B). Analysis of the spontaneous excitatory postsynaptic currents (sEPSCs) and long-term potentiation (LTP) of CA1 pyramidal neurons revealed no differences between WT and *Epm2a*$^{-/-}$ animals (Figures S8C and S8D).

i.c.v. administration of rAAV-h*EPM2A* vector reduces epileptic-like activity and restores physiological LTP in dentate gyrus granule cells

Analysis of granule cell membrane properties and current-voltage relationships showed no differences between WT and *Epm2a*$^{-/-}$ animals (Figures S9A–S9D). Treatment with the rAAV-h*EPM2A* vector did not alter the physiological properties of the granule cell membrane properties (Figures S9A–S9D). Analysis of the sEPSCs of dentate gyrus (DG) granule cells showed a trend toward a higher frequency of spontaneous events, normalized by the treatment (Figure S9E). In contrast, no differences were found between WT and *Epm2a*$^{-/-}$ animals in the amplitude of spontaneous events (Figure S9E). Using the electrophysiological technique of field potentials, we performed the analysis of elicited epileptic-like activity as described previously[42] on DG granule cells. The analysis showed increased epileptic-like activity in DG slices from rAAV-Null-injected *Epm2a*$^{-/-}$ mice compared with WT mice, as revealed by increased PS amplitude (Figure 7A). The rAAV-h*EPM2A* vector was able to completely reduce epileptic-like activity to the levels of WT animals (Figure 7A). Similarly, we found a complete inability of *Epm2a*$^{-/-}$ granule cells to perform LTP, as shown in Figure 7B. Hence, the rAAV-h*EPM2A* vector proved to be an excellent strategy to fully restore LTP as well (Figure 7B).

Expression of human laforin in the brain of *Epm2a*$^{-/-}$ mice led to significant changes in critical molecular pathways, as revealed by proteomic and phosphoproteomic analyses of the hippocampus

We performed a proteomic analysis, 3 months after injection, on tissue samples from the hippocampus of *Epm2a*$^{-/-}$-treated mice compared to *Epm2a*$^{-/-}$ and WT mice injected with the rAAV-Null vector. Given the pathophysiological characteristics of Lafora disease, our attention was focused on proteins involved in glycogen metabolism, oxidative stress and regulation of misfolded proteins, protein degradation via UPS, and neuronal hyperexcitability. Proteins that exhibited a Zq comparison with a p value less than 0.05 ($p < 0.05$) were classified as differentially abundant proteins (DAPs) in each respective comparison.

Epm2a$^{-/-}$ mice injected with the rAAV-Null vector exhibited an increased abundance of enzymes involved in glycogen metabolism, including GS, glycogenin (GYG), glycogen phosphorylase (PYGB/GP), and glycogen debranching (AGL/GDE), compared to the WT group (Figure 8A). Expression of human laforin reduced these levels in the hippocampus of *Epm2a*$^{-/-}$-treated mice (Figures 8A and 8B).

In *Epm2a*$^{-/-}$ mice injected with the rAAV-Null vector, a reduced abundance of proteins involved in protein folding and oxidative stress was observed, compared to WT mice. These proteins included binding immunoglobulin protein chaperone (HSPA5/binding immunoglobulin protein [BiP]), thioredoxin (TRX1), endoplasmic reticulum protein 29 (ERp29), selenoprotein W (SELENOW), and selenoprotein T (SELENOT) (Figure 8C). Remarkably, the expression of human laforin resulted in increased levels of these proteins (Figures 8C and 8D). Next, we explored whether the increased abundance of HSPA5/BiP, a participant in the unfolded protein response (UPR), was a consequence of the abundant release of exogenous laforin or a beneficial effect of laforin expression. To address this, we evaluated the interaction between this chaperone and the transmembrane stress sensor proteins inositol-requiring kinase 1 (IRE1) and PKR-related ER kinase (PERK). Coordinated protein response analysis revealed no significant changes in these proteins in *Epm2a*$^{-/-}$-treated mice compared to *Epm2a*$^{-/-}$ mice injected with rAAV-Null vector, 3 months after injection (Figures S11A and S11B), suggesting that the increase in proteins related to protein misfolding in the ER is likely a positive response to laforin expression.

Epm2a$^{-/-}$ mice injected with rAAV-Null also exhibited a decreased abundance of several E3 ubiquitin ligases, including tripartite motif-containing 33 (TRIM33); zinc and ring finger 2 (ZNRF2); and HECT, C2, and WW-domain containing E3 ubiquitin protein ligase 1 (HECW1), compared to WT mice (Figure 8E). Treatment with rAAV-h*EPM2A* led to an increased abundance of these proteins in the hippocampus of mice (Figures 8E and 8F). Notably, expression of human laforin increased the abundance of X-linked inhibitor of apoptosis (XIAP), an E3 ubiquitin ligase with anti-apoptotic function, and decreased the abundance of NEDD4-like E3 ubiquitin protein ligase (NEDD4.2), which has a role in the ubiquitination and endocytosis of GLT-1 in Lafora disease models (Figure 8F).

Epm2a$^{-/-}$ + rAAV-Null 60′, $p = 0.0168$) and 9 months after injection (F) (stereotyped movement counts: *Epm2a*$^{-/-}$ + rAAV-Null vs. WT + rAAV-Null 45′, $p = 0.0214$; *Epm2a*$^{-/-}$ + rAAV-Null vs. WT + rAAV-Null 60′, $p < 0.001$; *Epm2a*$^{-/-}$ + rAAV-h*EPM2A* vs. WT + rAAV-Null 60′, $p = 0.0040$. Rearing movement counts: *Epm2a*$^{-/-}$ + rAAV-Null vs. WT + rAAV-Null 45′, $p = 0.0497$; *Epm2a*$^{-/-}$ + rAAV-Null vs. WT + rAAV-Null 60′, $p = 0.0043$). Data are shown as mean (SD). One-way and two-way ANOVA tests with Tukey's multiple comparisons were performed between the experimental groups. *$p < 0.05$, **$p < 0.01$, ***$p < 0.001$, ****$p < 0.0001$, n.s., not significant. Asterisk indicates *Epm2a*$^{-/-}$ + rAAV-h*EPM2A* vs. *Epm2a*$^{-/-}$ + rAAV-Null; hash symbol (#) indicates WT + rAAV-Null vs. *Epm2a*$^{-/-}$ + rAAV-Null; dollar sign ($) indicates WT + rAAV-Null vs. *Epm2a*$^{-/-}$ + rAAV-h*EPM2A*. $n = 15$–25 mice per group and experiment.

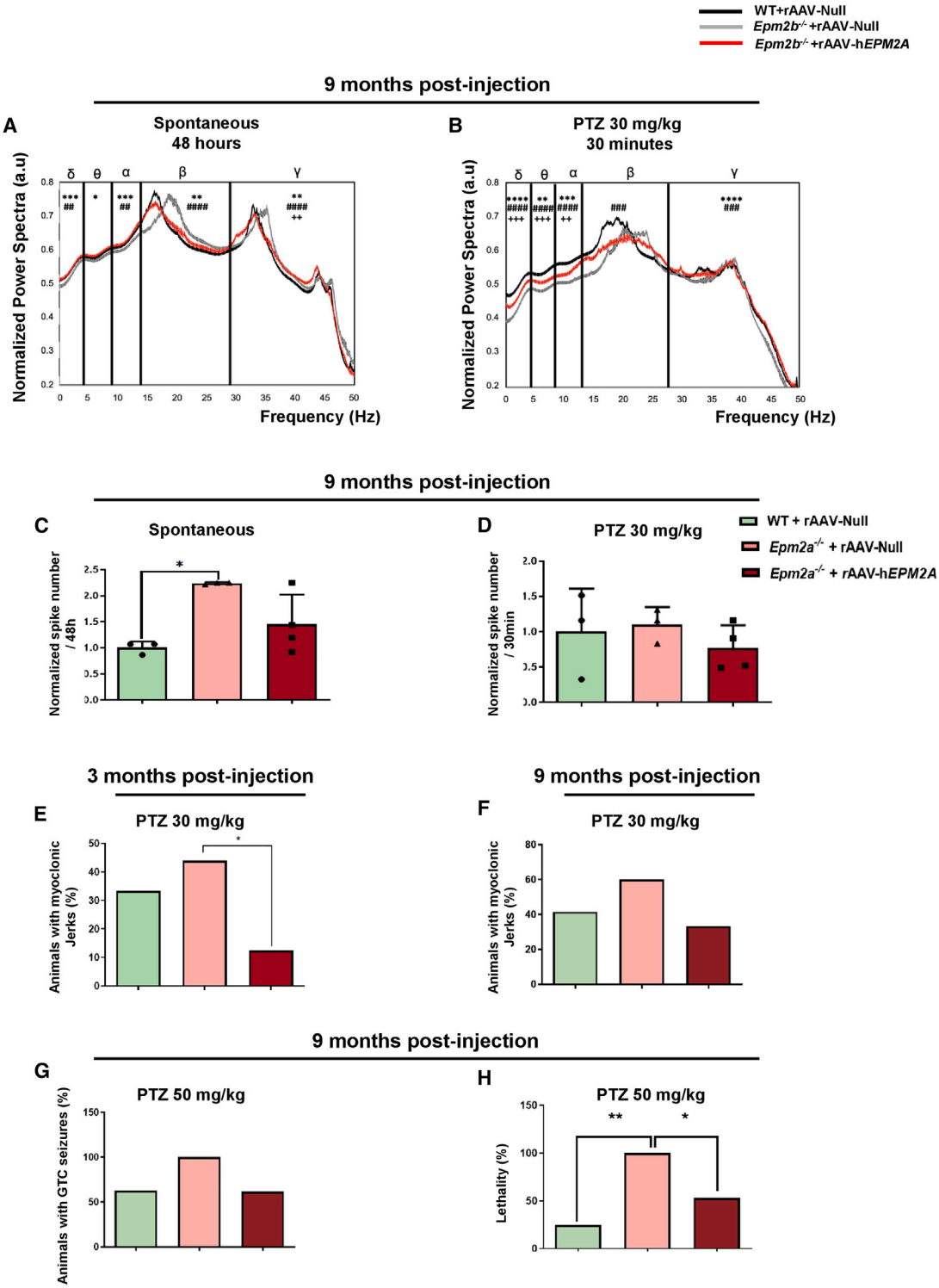

Figure 5. Analysis of EEG and susceptibility to PTZ in WT and *Epm2a*$^{-/-}$ mice 3 and 9 months after injection of rAAV-h*EPM2A* or rAAV-Null vectors

(A) Representative normalized power spectra were obtained from baseline EEG recordings (48 h). (B) Representative normalized power spectra obtained from EEG recordings after i.p. injection of PTZ at subconvulsive doses (30 mg/kg). Data are shown as mean ± SEM. A one-way ANOVA test with Tukey's multiple comparisons was performed between the AUC obtained after plotting the EEG powers of all experimental groups. Spontaneous: *Epm2a*$^{-/-}$ + rAAV-h*EPM2A* vs. *Epm2a*$^{-/-}$ + rAAV-Null delta and alpha frequency

(legend continued on next page)

Please cite this article in press as: Zafra-Puerta et al., Gene therapy for Lafora disease in the *Epm2a*$^{-/-}$ mouse model, Molecular Therapy (2024), https://doi.org/10.1016/j.ymthe.2024.05.032

In the hippocampus of 6-month-old *Epm2a*$^{-/-}$ mice injected with rAAV-Null, there was an increased abundance of proteins related to neuronal hyperexcitability (Figure 8G), including the glutamate ionotropic receptor α-amino-3-hydroxy-5-methyl-4-isoxazolepropionic acid (AMPA) type subunit 4 (GLUA4/GRIA4) and calcium voltage-gate channel auxiliary subunit gamma 8 (TARP γ-8). Conversely, there was a reduction in proteins such as glial γ-aminobutyric acid (GABA) transporter-2 (GAT-2) and potassium inwardly rectifying channel, subfamily J, member 10 (KIR4.1) compared to WT mice (Figure 8G). Expression of human laforin restored protein levels to those observed in WT mice (Figures 8G and 8H).

To analyze coordinated protein responses, a standardized log2 ratio, Zc, was calculated for some functional protein categories. In *Epm2a*$^{-/-}$-treated mice, we observed changes in relevant molecular pathways, which were not altered in the *Epm2a*$^{-/-}$ mouse model injected with rAAV-Null (Figures S10A and S10B). These signaling pathways include mammalian target of rapamycin (mTOR), RAP1 and RAS signaling cascades, epidermal growth factor (EGF)-induced KSR1-MEK-BRAF-ERK signaling, and phosphatidylinositol signaling system, which are downregulated (Figure S10A). Additionally, we found upregulated pathways related to the immune response and complement activation (Figure S10B).

Finally, we analyzed the levels of peptide phosphorylation in the hippocampus of 6-month-old *Epm2a*$^{-/-}$-treated mice compared to *Epm2a*$^{-/-}$ and WT mice injected with the rAAV-Null vector. The abundance of phosphorylated/dephosphorylated peptides was assessed using the standardized log2 ratio, Zp, for several proteins relevant to multiple molecular pathways in Lafora disease (Table S1). These included enzymes related to glycogen metabolism, such as GS, 1,4-alpha-glucan branching enzyme (GBE1), and PYGB/GP, and many kinases and phosphatases, such as RAC-beta serine/threonine-protein kinase (AKT2), AKT3, various protein kinase C (PKC) isoforms, phosphatidylinositol 3,4,5-trisphosphate 3-phosphatase and dual-specificity protein phosphatase (PTEN), kinase suppressor of RAS 1 (KSR1), and mitogen-activated protein kinase 7 (MAPK7). Differential phosphorylation was also observed in neurotransmitter receptors and channels, such as ionotropic glutamate receptor, NMDA2A, glutamate receptor (GRIA1), isoform 4 of glutamate receptor 2 (GRIA2), potassium voltage-gated channel subfamily KQT member 2 (KCNQ2), KCNQ3, and disc large homolog 1 or synapse-associated protein 97 (DLG1/SAP97) (Table S1), all of which may be involved in the molecular mechanisms underlying Lafora disease.

Expression of human laforin in the hippocampus of *Epm2a*$^{-/-}$ mice led to a decrease in GS and an increase in HSPA5/BiP expression, validating the proteomic results

To validate some of the most relevant findings observed by proteomic analysis, we examined the levels of GS and BiP expression by immunohistochemistry (IHC) in the hippocampus of *Epm2a*$^{-/-}$ mice 3 months post injection (Figure S12). Consistent with the findings of the proteomic analysis, we found that the hippocampus of treated *Epm2a*$^{-/-}$ mice exhibited lower levels of GS expression compared to the levels present in the hippocampus of *Epm2a*$^{-/-}$ mice injected with the rAAV-Null vector (Figures S12A and S12B). Furthermore, also in agreement with the findings revealed by proteomic analysis, we observed that the levels of the chaperone HSPA5/BiP in the CA2 region of the hippocampus of *Epm2a*$^{-/-}$ mice treated with rAAV-h*EPM2A* were significantly higher than that in *Epm2a*$^{-/-}$ mice injected with the rAAV-Null vector (Figures S12C and S12D).

DISCUSSION

This study demonstrates the significant therapeutic impact of a gene therapy in a mouse model of Lafora disease. This is the first-ever example of a successful gene therapy with enduring benefits in a preclinical mouse model of Lafora disease. We developed a gene therapy with an rAAV2/9 vector to restore the expression of the *EPM2A* gene and recover the function of laforin in the *Epm2a*$^{-/-}$ mouse model of Lafora disease. Evaluation of the effects of this form of therapy involved testing memory abilities, motor coordination, spontaneous locomotor activity, epileptic activity, and neuronal hyperexcitability, along with neuropathological and molecular changes. Treatment with the rAAV-h*EPM2A* vector improved many neurological outcomes 3 and 9 months after a single i.c.v. injection. Proteomic and phosphoproteomic analysis revealed changes in important molecular

waves $p < 0.001$, theta frequency waves $p = 0.0104$, beta frequency waves $p = 0.0026$, and gamma frequency waves $p = 0.0067$; WT + rAAV-Null vs. *Epm2a*$^{-/-}$ + rAAV-Null delta frequency waves $p = 0.0014$, alpha frequency waves $p = 0.0040$, and beta and gamma frequency waves $p < 0.001$; WT + rAAV-Null vs. *Epm2a*$^{-/-}$ + rAAV-h*EPM2A* gamma frequency waves $p = 0.0041$. PTZ injection: *Epm2a*$^{-/-}$ + rAAV-h*EPM2A* vs. *Epm2a*$^{-/-}$ + rAAV-Null delta, alpha, and gamma frequency waves $p < 0.001$, theta frequency waves $p = 0.0073$; WT + rAAV-Null vs. *Epm2a*$^{-/-}$ + rAAV-Null delta, theta, alpha, beta, and gamma frequency waves $p < 0.001$; WT + rAAV-Null vs. *Epm2a*$^{-/-}$ + rAAV-h*EPM2A* delta and theta frequency waves $p < 0.001$, and alpha frequency waves $p = 0.0088$. $^{*}p < 0.05$, $^{**}p < 0.01$, $^{***}p < 0.001$, $^{****}p < 0.000.1$. Asterisk indicates *Epm2a*$^{-/-}$ mice treated with rAAV-h*EPM2A* vs. *Epm2a*$^{-/-}$ mice injected with rAAV-Null; hash symbol (#) indicates WT injected with rAAV-Null vs. *Epm2a*$^{-/-}$ mice injected with rAAV-Null; plus sign (+) indicates WT injected with rAAV-Null vs. *Epm2a*$^{-/-}$ mice treated with rAAV-h*EPM2A*. $n = 3$–4 mice per group. (C and D) Analysis of spontaneous (C) and PTZ-induced (D) IEDs. A non-parametric Kruskal-Wallis test was performed followed by Dunn's multiple comparisons. Data are shown as normalized mean ± SD. Values were normalized using WT mice injected with rAAV-Null values. Spontaneous: WT + rAAV-Null vs. *Epm2a*$^{-/-}$ + rAAV-Null, $p = 0.0447$. $n = 3$–4 mice per group. $^{*}p < 0.05$, $^{**}p < 0.01$, $^{***}p < 0.001$, $^{****}p < 0.000.1$. (E and F) Percentage of animals with myoclonic jerks after i.p. injection of 30 mg/kg PTZ in WT and *Epm2a*$^{-/-}$ mice 3 months (*Epm2a*$^{-/-}$ + rAAV-Null vs. *Epm2a*$^{-/-}$ + rAAV-h*EPM2A*, $p = 0.0255$) (E) and 9 months (F) after injection. (G) Percentage of animals with GTC seizures, and (H) percentage of lethality after i.p. injection of 50 mg/kg PTZ in WT and *Epm2a*$^{-/-}$ mice 9 months after i.c.v. administration of rAAV-h*EPM2A* or rAAV-Null. WT + rAAV-Null vs. *Epm2a*$^{-/-}$ + rAAV-Null, $p = 0.0070$; *Epm2a*$^{-/-}$ + rAAV-h*EPM2A* vs. *Epm2a*$^{-/-}$ + rAAV-Null, $p = 0.0468$. Data are shown as percentages. A Fisher's exact test was performed between the experimental groups. $^{*}p < 0.05$, $^{**}p < 0.01$. $n = 15$–25 mice per group and experiment.

Please cite this article in press as: Zafra-Puerta et al., Gene therapy for Lafora disease in the *Epm2a*$^{-/-}$ mouse model, Molecular Therapy (2024), https://doi.org/10.1016/j.ymthe.2024.05.032

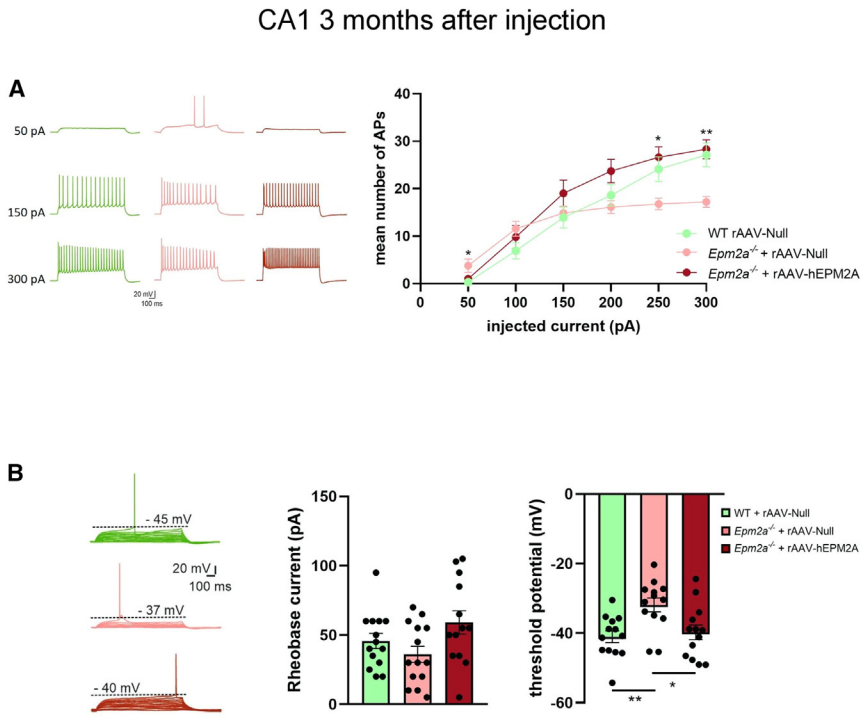

Figure 6. Action potential discharge of CA1 pyramidal neurons from WT and *Epm2a*$^{-/-}$ mice after injection of rAAV-h*EPM2A* or rAAV-Null vectors

(A and B) (A) AP firing patterns in response to 50-pA stepped depolarizing current injections (duration 1,200 ms) from CA1 pyramidal neurons in WT (green trace) and *Epm2a*$^{-/-}$ mice injected with either rAAV-Null (pink trace) or rAAV-h*EPM2A* (red trace) vectors. The plot shows mean (±SEM) number of APs at the different input currents (n = 10 neurons for WT, n = 9 for *Epm2a*$^{-/-}$ + rAAV-Null, n = 10 for *Epm2a*$^{-/-}$ + rAAV-h*EPM2A*; 50 pA, WT vs. *Epm2a*$^{-/-}$ + rAAV-Null p = 0.0207; 250 pA, WT vs. *Epm2a*$^{-/-}$ + rAAV-Null, p = 0.0176; 300 pA, WT vs. *Epm2a*$^{-/-}$ + rAAV-Null, p = 0.0019). A student's t test was performed. *p < 0.05, **p < 0.01. (B) Example current-clamp recordings (5-pA stepped depolarizing current injections; 50 ms), scaled to show the AP threshold, in CA1 pyramidal neurons of WT (green), *Epm2a*$^{-/-}$ + rAAV-Null (pink), and *Epm2a*$^{-/-}$ + rAAV-h*EPM2A* (red) mice. The plots show similar rheobase current (left) for the three groups (WT, 45.71 ± 5.6 pA, n = 14; *Epm2a*$^{-/-}$ + rAAV-Null, 36.07 ± 5.8 pA, n = 14; *Epm2a*$^{-/-}$ + rAAV-h*EPM2A*, 59.08 ± 8.4 pA, n = 13) while AP threshold (right) of *Epm2a*$^{-/-}$ + rAAV-Null is significantly depolarized with respect to WT (WT, −41.01 ± 1.7 mV, n = 13; *Epm2a*$^{-/-}$ + rAAV-Null, −31.87 ± 2 mV, n = 13; WT vs. *Epm2a*$^{-/-}$ + rAAV-Null, p = 0.0020). A student's t test was performed. **p < 0.01. Note that injection of rAAV-h*EPM2A* vector rescues the AP threshold of *Epm2a*$^{-/-}$ mice to control values (*Epm2a*$^{-/-}$ + rAAV-Null, −31.87 ± 2 mV, n = 13; *Epm2a*$^{-/-}$ + rAAV-h*EPM2A*, −39.74 ± 2.1 mV, n = 13; *Epm2a*$^{-/-}$ + rAAV-Null vs. *Epm2a*$^{-/-}$ + rAAV-h*EPM2A*, p = 0.0131). A student's t test was performed. *p < 0.05. Data are reported as means ± SEM.

signaling pathways associated with the expression of human laforin, suggesting possible molecular pathways through which human laforin could produce the observed beneficial effects.

Disruption of either laforin or malin results in the formation of aggregates of polyglucosans.[14–17] In our study, we observed a significant reduction in LB formation in *Epm2a*$^{-/-}$-treated mice compared to mice injected with rAAV-Null. The laforin-malin complex controls glycogen synthesis by causing the proteasome-dependent degradation of GS, GDE, and PTG.[11,12] Proteomic analysis revealed that untreated *Epm2a*$^{-/-}$ mice exhibited an abnormal abundance of these enzymes involved in glycogen metabolism in the hippocampus compared to WT mice. Gene therapy reversed this enzymatic imbalance, restoring enzyme levels to those observed in WT mice, thus correcting abnormal glycogen accumulation and LB formation.

Furthermore, besides the formation of LBs, which sequester a variety of proteins involved in proteostasis and autophagy,[22,43,44] disruptions in the laforin-malin complex lead to the generation of misfolded proteins, coupled with dysfunctions in the UPS and autophagy pathways. These pathophysiological conditions result in heightened ER stress.[13,19,22,45–48] These anomalies are further exacerbated by issues related to mitochondrial functionality, following reactive oxygen species (ROS) production, and challenges in counteracting these reactive species due to disruptions in antioxidant mechanisms.[18,49–51] Cumulatively, along with the diminished glutamate reuptake capacity of astrocytes and its accumulation within the synaptic cleft described in murine models of Lafora disease,[52–54] this results in a notable surge in astrogliosis, neuroinflammation, and neuronal hyperexcitability,[52,53,55–59] ultimately leading to apoptosis and neurodegeneration.[20] Our investigation showed a marked reduction in neuroinflammation following i.c.v. injection of the rAAV-h*EPM2A* vector, observed both 3 and 9 months post injection across various hippocampal regions and in layers IV–V of the sensorimotor cortex in *Epm2a*$^{-/-}$ mice. Furthermore, a significant decline in active caspase-3 levels and a modest increase in neuron count were noted in the CA1 region of the hippocampus in these mice 3 months post-i.c.v. administration.

Chaperones,[25,60] antioxidants,[25,27] and autophagy stimulators[24,25,61] are examples of compounds that have shown promise in lowering or rescuing neuroinflammation in Lafora disease mouse models. In this regard, our proteomic analysis revealed a substantial increase in the abundance of proteins associated with protein folding, UPS, and the regulation of ROS in *Epm2a*$^{-/-}$-treated mice. Thus, the abundances of TRX1, an antioxidant and proteasome-related protein that is decreased in fibroblasts from Lafora disease patients,[62] and BiP chaperone[19] are increased in *Epm2a*$^{-/-}$-treated mice. The ERp29 chaperone and the antioxidant selenoproteins T and W are also more abundant in *Epm2a*$^{-/-}$-treated mice. Furthermore, rAAV-h*EPM2A* increased the abundance of several E3 ubiquitin ligases.

Please cite this article in press as: Zafra-Puerta et al., Gene therapy for Lafora disease in the *Epm2a*$^{-/-}$ mouse model, Molecular Therapy (2024), https://doi.org/10.1016/j.ymthe.2024.05.032

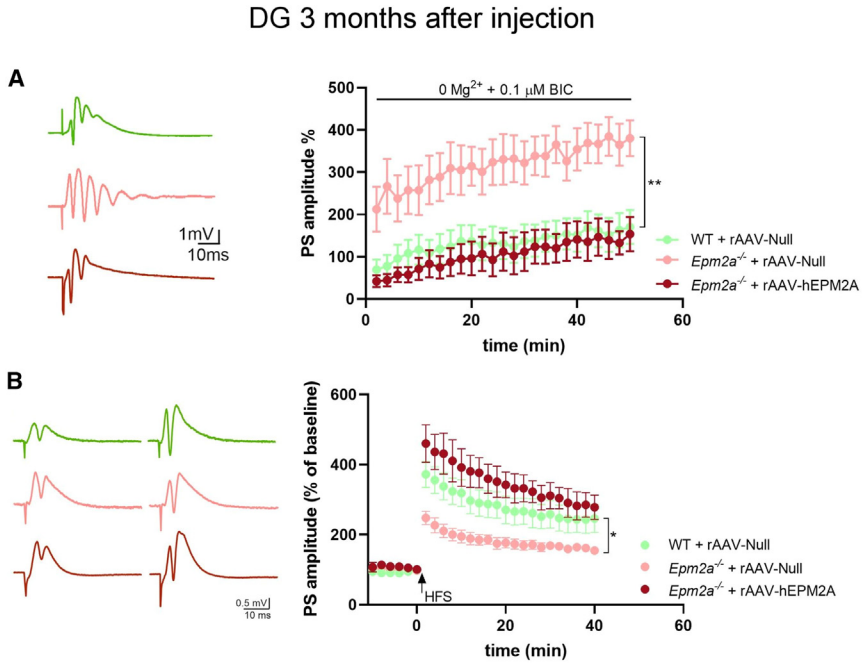

Figure 7. Epileptic-like activity and LTP in DG slices of WT and *Epm2a*$^{-/-}$ mice after injection of rAAV-h*EPM2A* or rAAV-Null vectors

(A and B) Representative traces of field potentials (FPs) and time course graph of population spikes (PS) amplitude recorded in the DG of WT (green), *Epm2a*$^{-/-}$ + rAAV-Null (pink), and *Epm2a*$^{-/-}$ + rAAV-h*EPM2A* (red) mice in a magnesium-free artificial cerebrospinal fluid (ACSF) in the presence of 0.1 μM bicuculline, showing a time-dependent increase of the epileptic-like activity in *Epm2a*$^{-/-}$ + rAAV-Null mice compared to WT (WT, 170.1% ± 39.9%, n = 9; *Epm2a*$^{-/-}$ + rAAV-Null, 380.3% ± 42.5%, n = 10; WT vs. *Epm2a*$^{-/-}$ + rAAV-Null, p = 0.0085). A two-way ANOVA test was performed. $^{**}p < 0.01$. Note that injection of rAAV-h*EPM2A* vector rescues the epileptic-like activity to control values (WT, 170.1% ± 39.9%, n = 9; *Epm2a*$^{-/-}$ + rAAV-h*EPM2A*, 153.6% ± 40.6%, n = 8). (B) Representative PS traces recorded before (left) and 40 min after (right) the HFS protocol in DG slices of WT (green), *Epm2a*$^{-/-}$ + rAAV-Null (pink), and *Epm2a*$^{-/-}$ + rAAV-h*EPM2A* (red) mice. The time-course plot of PS amplitudes recorded in the DG before and after HFS protocol shows a significative impairment of LTP in *Epm2a*$^{-/-}$ + rAAV-Null mice compared to WT (WT, 246.4% ± 40.3%, n = 7; *Epm2a*$^{-/-}$ + rAAV-Null, 155.0% ± 11.3%, n = 6; WT vs. *Epm2a*$^{-/-}$ + rAAV-Null, p = 0.0350). A two-way ANOVA test was performed. $^{*}p < 0.05$. Note that injection of rAAV-h*EPM2A* vector rescues LTP to physiological levels (WT, 246.4% ± 40.3%, n = 7; *Epm2a*$^{-/-}$ + rAAV-hEPM2A, 278.2% ± 34.7%, n = 5). Data are reported as means ± SEM.

However, NEDD4-2 ubiquitin ligase, which has previously been reported to induce the ubiquitination and endocytosis of GLT-1 in Lafora disease models,[54] exhibits lower abundance. The reduction in the abundance of this protein could produce decreased ubiquitination of GLT-1, increasing the levels of the glutamate transporter at the plasma membrane and the glutamate uptake capacity.[54,63] These data strongly suggest that the expression of laforin in treated mice improves neurological functions by reducing misfolded proteins, stimulating UPS and glutamate reuptake, and alleviating alterations in ROS. Consequently, this leads to a decrease in neuroinflammation and cell death, ultimately correcting neurological alterations in memory abilities, spontaneous motor activity, and motor coordination. Strangely, for unknown reasons, although our group of *Epm2a*$^{-/-}$ animals injected with rAAV-Null vector showed memory deficits 3 months after injection of the rAAV-Null vector and these were reduced with rAAV-h*EPM2A* treatment, their memory failures were absent 9 months after injection. Therefore, we could not evaluate the treatment with rAAV-h*EPM2A* vector in memory performance 9 months after treatment administration.

Mice treated with rAAV-h*EPM2A* showed fewer myoclonic jerks and GTC seizures and a lower mortality after i.p. administration of both subconvulsive and convulsive PTZ doses. Furthermore, video-EEG analysis revealed that *Epm2a*$^{-/-}$-treated mice exhibited a restoration of normal power spectra, particularly in the gamma range, which is known to be associated with epileptic activity,[64–66] as well as a reduced number of IEDs. *Epm2a*$^{-/-}$-treated mice displayed less decrease in EEG power after PTZ administration across high-frequency waves, indicating decreased PTZ susceptibility.[67]

Our electrophysiological findings reveal region-specific impairments within the hippocampus of *Epm2a*$^{-/-}$ mice, particularly highlighting intrinsic hyperexcitability in CA1 pyramidal neurons. Indeed, our analysis indicates that *Epm2a*$^{-/-}$ mice injected with rAAV-Null exhibit an increased mean number of APs elicited in pyramidal neurons in response to small depolarizing current steps compared to their WT and *Epm2a*$^{-/-}$ mice treated with rAAV-h*EPM2A* counterparts. Furthermore, CA1 neurons from *Epm2a*$^{-/-}$ mice injected with rAAV-Null showed a reduced ability to maintain firing rates when faced with increasing current injections, unlike their WT and *Epm2a*$^{-/-}$ mice treated with rAAV-h*EPM2A* counterparts. This phenomenon of rapidly declining firing performance has been similarly observed in models of aging and various neurodegenerative disorders, as reported previously.[68] These results highlight that treatment with rAAV-h*EPM2A* reverts the intrinsic hyperexcitability in CA1 pyramidal neurons. Moreover, we have observed that treatment with rAAV-h*EPM2A* reverses the enhanced epileptic-like activity to WT conditions and restores detrimental LTP in the DG of *Epm2a*$^{-/-}$ mice injected with rAAV-Null.

Given that the rAAV-h*EPM2A* vector preferably transduces CA1 neurons, improvements in the neuronal function of the DG could

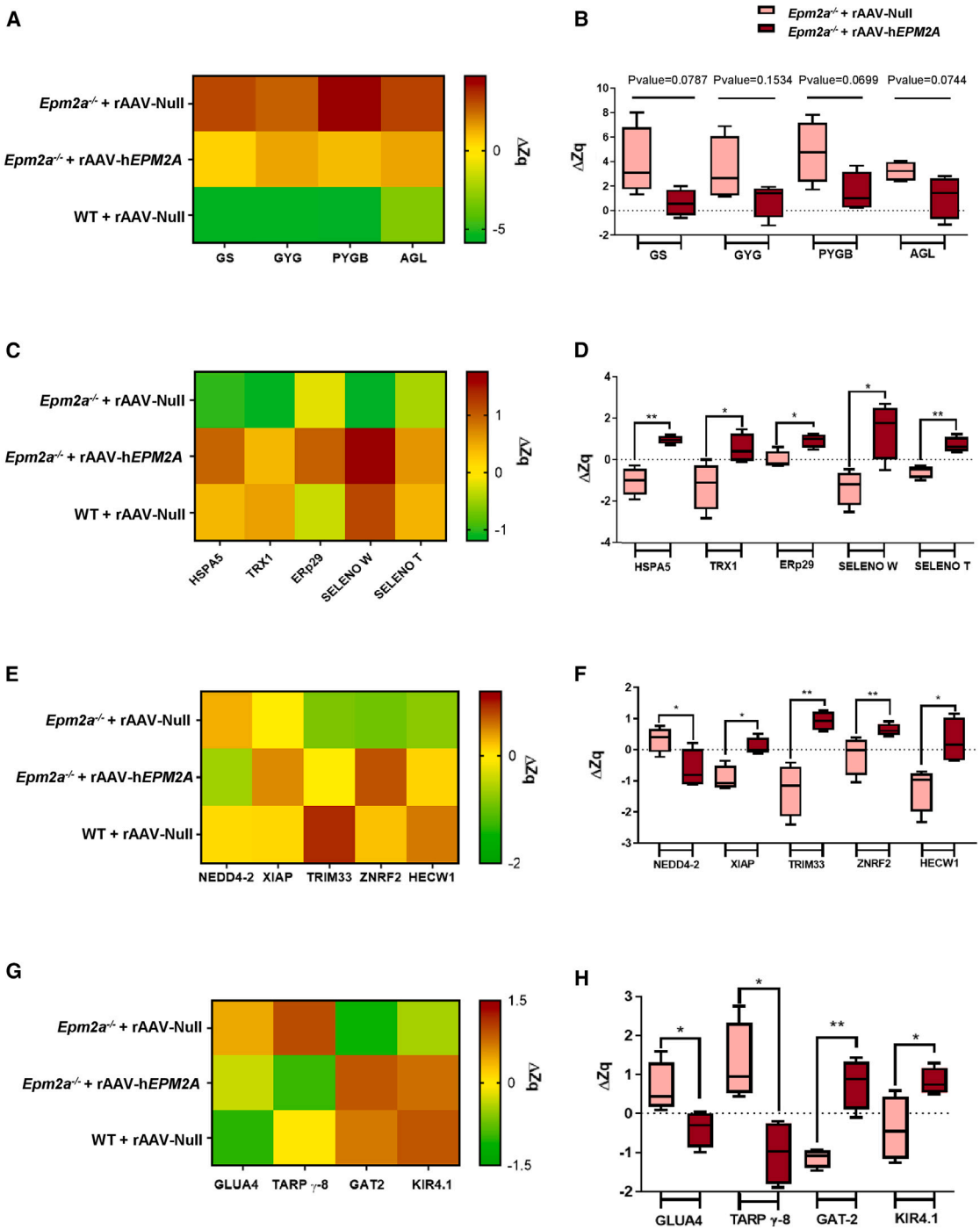

Figure 8. Variations in the abundance of proteins in the hippocampus of WT and *Epm2a*$^{-/-}$ mice 3 months after i.c.v. injection of rAAV-h*EPM2A* or rAAV-Null vectors

(A) Heatmap representing differences in the abundance of proteins (ΔZq) involved in glycogen metabolism between WT + rAAV-Null, *Epm2a*$^{-/-}$ + rAAV-h*EPM2A* and *Epm2a*$^{-/-}$ + *rAAV-Null.* (B) Box plot showing the differences in the abundance of proteins involved in glycogen metabolism between *Epm2a*$^{-/-}$ + rAAV-h*EPM2A* and *Epm2a*$^{-/-}$ + rAAV-Null. (C) Heatmap representing variations in the protein abundance related to proteostasis and reactive oxygen species (ROS) regulation between WT + rAAV-Null, *Epm2a*$^{-/-}$ + rAAV-h*EPM2A* and *Epm2a*$^{-/-}$ + rAAV-Null. (D) Box plots showing variations in the protein abundance related to proteostasis and ROS regulation between *Epm2a*$^{-/-}$ + rAAV-h*EPM2A* and *Epm2a*$^{-/-}$ + rAAV-Null. *Epm2a*$^{-/-}$ + rAAV-h*EPM2A* vs. *Epm2a*$^{-/-}$ + rAAV-Null: HSPA5 $p = 0.0013$, TRX1 $p = 0.0385$, ERp29 $p = 0.0130$, SELENO W $p = 0.0143$, and SELENO T $p = 0.0021$. (E) Heatmap representing differences in the abundance of proteins involved in protein degradation through

(legend continued on next page)

Please cite this article in press as: Zafra-Puerta et al., Gene therapy for Lafora disease in the *Epm2a*$^{-/-}$ mouse model, Molecular Therapy (2024), https://doi.org/10.1016/j.ymthe.2024.05.032

be achieved through functional enhancements in the CA1-DG axis, related to memory consolidation.[69,70] These electrophysiological changes corroborate the behavioral and epileptic analyses, which showed that treatment reduces sensitivity to PTZ, normalizes EEG profiles, and corrects cognitive deficits in these mice.

Alterations in ionotropic receptor expression, trafficking, subunit composition, and biophysical properties might disrupt information transmission, contributing to both hyperexcitability and synaptic plasticity issues.[71] Other changes consistent with EEG, PTZ sensitivity, and electrophysiological alterations were noted in proteomic and phosphoproteomic studies. A higher abundance of the GABA transporter GAT-2 was observed in the hippocampus of mice treated with the therapeutic vector. Reduced GAT-2 levels have been associated with temporal lobe epilepsy.[72] This GABA transporter may contribute to reducing neuronal hyperexcitability in treated mice through glutamate-induced GABA release.[73–75] Phosphorylation of *N*-methyl-D-aspartate (NMDA) modulatory subunits (NR1, NR2A, and NR2B) and AMPA receptors regulates neuronal excitability, among other neuronal pathways. In the hippocampus of mice treated with rAAV-h*EPM2A*, we observed significant dephosphorylation of NR2A and AMPAR subunits GLUA1 and GLUA2, along with a notable decrease in GLUA4 abundance. These findings suggest that gene therapy with rAAV-h*EPM2A* may decrease neuronal hyperexcitability by reducing glutamatergic transmission.

In addition, we observed a reduction in neuronal hyperexcitability resulting from molecular pathways beyond the glutamatergic and GABAergic systems. Potassium channels are crucial for maintaining the balance of brain excitability. Thus, treated mice exhibited restoration of normal KIR4.1 channel abundance. Additionally, mutations in KCNQ2 and KCNQ3 are linked to benign familial neonatal convulsions (BFNCs), and phosphorylation of these channels by cyclic AMP (cAMP)-dependent protein kinase (PKA) stimulates their activity, reducing epileptic activity.[76,77] Phosphorylation patterns suggest increased PKA activity in mice treated with therapeutic vectors, with higher phosphorylation of KCNQ2 and KCNQ3 in the hippocampus. These findings may collectively explain the decrease in epileptic activity in *Epm2a*$^{-/-}$-treated mice.

Proteomic studies revealed changes in different pathways not previously associated with Lafora disease, including mTOR, RAP1, RAS, KSR1-MEK-BRAF-ERK, and phosphatidylinositol signaling pathways. Interestingly, the phosphatidylinositol 3-kinase (PI3K)/AKT/mTOR signaling pathway has been observed to be elevated in the brains of patients with epilepsy in various genetic and acquired epilepsy models *in vivo* and in laforin-deficient cells.[11,78] This pathway plays a role in controlling processes related to seizures, synaptic plasticity, cell growth, and ion channel protein expression, which potentially contribute to epileptogenesis.[11,79] Although not previously described in Lafora disease, human laforin may reduce epileptogenic activity in *Epm2a*$^{-/-}$ mice by regulating proteins within the PI3K/AKT/mTOR pathway through its protein phosphatase activity. Furthermore, pathways associated with immune response and complement activation may experience an increase in activity due to rAAV-h*EPM2A*-induced laforin expression in *Epm2a*$^{-/-}$ mice.

In conclusion, our study demonstrates that gene therapy inducing laforin expression with the coding region of the human *EPM2A* gene results in significant neurological improvements in a mouse model of Lafora disease. Treatment at an early symptomatic stage markedly reduced neuroinflammation and LB formation, delayed memory and motor alterations, improved motor coordination, and reduced epileptic activity and electrophysiological impairments. Furthermore, proteomic and phosphoproteomic analyses shed light on various mechanisms through which laforin may be inducing these improvements, indicating potential new targets in Lafora disease. Our results with gene therapy open a new avenue for treating this devastating disease.

MATERIALS AND METHODS

Experimental animals

We used the *Epm2a*$^{-/-}$ mouse model of Lafora disease, generated following previously described methods,[21] and age-matched WT mice (C57BL6). Since no-gender-related phenotype differences have been described in mice[80] or patients with Lafora disease,[26,81] we analyzed data from male and female mice indistinctively. The mouse colonies were bred in the Animal Facility Service of the Instituto de Investigación Sanitaria-Fundación Jiménez Díaz and were housed in isolated cages in ventilated racks with a 12:12 light/dark cycle at a constant temperature of 23°C, with free access to food and water. All experiments were conducted with the utmost care to use and sacrifice the minimum number of animals while minimizing their suffering. The experimental procedures adhered to the "Principles of Laboratory Animal Care" (NIH publication no. 86–23, revised 1985), as well as the European Communities Council Directive (2010/63/EU) and were approved by the Ethical Review Board of the Instituto de Investigación Sanitaria-Fundación Jiménez Díaz and by the Animal Care and Use Committee at the University of Perugia (authorization no. 2B818.N.9JX).

UPS between WT + rAAV-Null, *Epm2a*$^{-/-}$ + rAAV-h*EPM2A* and *Epm2a*$^{-/-}$ + rAAV-Null. (F) Box plots showing differences in the abundance of proteins involved in protein degradation through UPS between *Epm2a*$^{-/-}$ + rAAV-h*EPM2A* and *Epm2a*$^{-/-}$ + rAAV-Null.. *Epm2a*$^{-/-}$ + rAAV-h*EPM2A* vs. *Epm2a*$^{-/-}$ + rAAV-Null: NEDD4-2 $p = 0.0406$, TRIM33 $p = 0.0058$, ZNRF2 $p = 0.0026$, XIAP $p = 0.0485$, and HECW1 $p = 0.0269$. (G) Heatmap representing variations in the abundance of proteins associated with neuronal excitability between WT + rAAV-Null, *Epm2a*$^{-/-}$ + rAAV-h*EPM2A* and *Epm2a*$^{-/-}$ + rAAV-Null. (H) Box plots showing variations in the abundance of proteins associated with neuronal excitability between *Epm2a*$^{-/-}$ + rAAV-h*EPM2A* and *Epm2a*$^{-/-}$ + rAAV-Null. *Epm2a*$^{-/-}$ + rAAV-h*EPM2A* vs. *Epm2a*$^{-/-}$ + rAAV-Null: GLUA4 $p = 0.0432$, TARP γ-8 $p = 0.0139$, GAT2 $p = 0.0015$, and KIR4.1 $p = 0.0351$. Data are shown as means of a standardized log2 ratio at the protein level (Zq). Whiskers in box plots show the minimum and maximum values. A t test was carried out between the experimental groups. $^{*}p < 0.05$, $^{**}p < 0.01$. $n = 4$ mice per group.

Production of rAAV2/9-CAG-h*EPM2A*, rAAV2/9-CAG-*GFP*, and rAAV2/9-CAG-Null vectors

The rAAV2/9-CAG-h*EPM2A* (rAAV-h*EPM2A*) vector, containing the cDNA of the *EPM2A* gene transcript variant 1 (h*EPM2A*) (GeneBank: NM_005670.4); the rAAV2/9-CAG-Null (rAAV-Null) vector, containing a non-coding DNA; and the rAAV2/9-CAG-*GFP* (rAAV-*GFP*) vector, containing the green fluorescent protein (*GFP*) gene, were generated in the Unitat de Producció de Vectors (UPV; www.viralvector.eu). The production of those vectors was performed following the triple transfection system: (1) the ITR-containing plasmid, (2) the plasmid encoding AAV capsid (VP1, VP2, and VP3 proteins) and replicate genes, and (3) the adenoviral helper plasmid. To remove empty capsids, AAV vectors were purified by iodixanol-based ultracentrifugation.[82]

Stereotaxic intracerebroventricular injections

Three-month-old *Epm2a*$^{-/-}$ mice received a single i.c.v. injection of rAAV-h*EPM2A*, rAAV-*GFP*, or rAAV-Null vectors. Mice were anesthetized in an induction chamber filled with 4% isoflurane and 2% O_2 and maintained with 2% isoflurane and 1.5% O_2. Mice were fixed in a stereotaxic frame (Stoelting, Illinois, USA) and body temperature was maintained using a heating pad at 37°C. Hydration was controlled with a subcutaneous saline injection (1 mL), and ophthalmic gel was applied to prevent dry eyes. The total number of mice subjected to rAAV-h*EPM2A* and rAAV-Null i.c.v. injections was 25–35 per group and condition.

The incision site was sterilized with 70% ethanol and was made in the midline, starting behind the eyes. Bregma and lambda were identified with H_2O_2 on the skull. A small burr hole was drilled according to stereotaxic coordinates of the right cerebral lateral ventricle relative to bregma (anterioposterior −0.3 and mediolateral −0.9). A Hamilton syringe (Thermo Fisher Scientific, MA, USA, catalog #10664301) was introduced at −2.5 cm in the dorsoventral axis to deliver 3 μL of viral suspension with a titer of 1.26 – 10^{12} vg/mL at a rate of 1 μL/min. The incision was sutured, and meloxicam (Boehringer Ingelheim, Georgia, USA) (5 mg/kg) was administered as an analgesic.

RNA extraction and RT-qPCR

RNA was extracted from brain samples previously homogenized on ice with TRIzol Reagent (Thermo Fisher Scientific, MA, US). The RNA pellets were washed, dried, resuspended, -treated with DNase Enzyme (Thermo Fisher Scientific, MA, US), and quantified with a NanoDrop ND-1000 spectrophotometer (Thermo Fisher, MA, US). RT-PCR experiments were carried out using the High-Capacity cDNA Reverse Transcription Kit with RNase inhibitor (Thermo Fisher Scientific, MA, US) with 1 μg of RNA per reaction. The RT-PCR conditions were 25°C for 10 min, 37°C for 120 min, and 85°C for 5 min. For RT-qPCR, cDNA from the h*EPM2A* transcript variant 1 was used as a template. The reaction was performed with TaqMan Fast Advanced Master Mix (Thermo Fisher Scientific, MA, USA), with *Epm2a*, *EPM2A*, and *Gapdh* probes (Thermo Fisher Scientific, MA, USA). The qPCR conditions were 50°C for 2 min, 95°C for 2 min, 95°C for 1 s, and 60°C for 20 s (40 cycles). Analysis was performed using the $2^{-\Delta\Delta CT}$ method.

Immunofluorescence, IHC, and PAS-D staining

Mice were anesthetized and transcardially perfused with 4% phosphate-buffered paraformaldehyde, and their brains were removed, dehydrated, and paraffin embedded. Blocks were then sectioned into 5-μm-thick consecutive sections. For PAS-D staining, sections were rehydrated using decreasing graded alcohols, treated with porcine pancreas α-amylase (5 mg/mL in dH_2O) (Merck, Darmstadt, Germany), and processed with the PAS Kit (Merck, Darmstadt, Germany). Following this, they were counterstained with Gill no. 3 hematoxylin (Merck, Darmstadt, Germany). For paraffin IHC and immunofluorescence (IF-P), rehydrated sections underwent boiling in 0.1 M sodium citrate buffer, pH 6.0. Samples were then incubated in blocking buffer (1% bovine serum albumin, 5% fetal bovine serum, 2% Triton X-100, diluted in PBS) and then with primary antibodies diluted in blocking buffer. For IHC, the primary antibodies used were GFP (1:100 dilution; Abcam, Cambridge, UK; catalog #ab183734), ionized calcium-binding adapter molecule 1 antibody (Iba1) (1:100 dilution; Thermo Fisher Scientific, MA, USA; #MA536257), NeuN (1:100 dilution; Millipore, Temecula, CA, USA; catalog # MAB377), GFAP (1:1,000 dilution; Millipore, Temecula, CA, USA; catalog #MAB360), laforin (3 μg/mL; Lifespan Biosciences, WA, US, catalog #LS B6474), GS (1:100 dilution; Abcam, Cambridge, U.K.; catalog #EP817Y), BiP chaperone (1:1,000 dilution; Millipore, Temecula, CA, USA.; catalog # MABC675), and cleaved caspase-3 (1:400 dilution; Cell Signaling Technology, Danvers, MA, USA.; catalog #9661). Sections were stained with the Vectastain ABC kit (Vector Laboratories, Burlingame, CA, USA). Immunoreactivity was revealed using diaminobenzidine (Dako Cytomation, CA, USA) and H_2O_2 and counterstained with Carazzi hematoxylin (Panreac Quimica, Barcelona, Spain). For IF-P, the primary antibody was GFAP (1:1,000 dilution; Millipore, Temecula, CA, USA; catalog #MAB360), NeuN (1:100 dilution; Millipore, Temecula, CA, USA; catalog # MAB377), and laforin (3 μg/mL; Lifespan Biosciences, WA, US, catalog #LS B6474). Secondary antibodies were conjugated to Alexa Fluor 594 (donkey anti-mouse, 1:400 dilution; Abcam, Cambridge, UK, catalog #ab150108). Samples from four to six mice per group were used, and two consecutive sections per animal were stained and analyzed. Images from the different areas of the hippocampus were acquired using a Leica DMLB 2 microscope (Leica, Wetzlar, Germany) connected to a Leica DFC320 FireWire digital microscope camera (Leica, Wetzlar, Germany) for IHC-processed sections, and with a Zeiss Axioscope 5 (Zeiss, Jena, Germany) connected to an Axiocam 208 color camera (Zeiss, Jena, Germany) for sections processed via IF-P. Subsequently, LBs and NeuN-, Iba1-, and GFAP- positive cells were quantified by two researchers using ImageJ software (NIH, Bethesda, MD, USA). GS expression levels were quantified by measuring the percentage of stained area with ImageJ and Fiji (2.15.0). Reported values represent the average of these quantifications.

Object recognition task

The object recognition task (ORT) was used to assess episodic memory retention. Mice were individually familiarized with a dark box in an open field for 10 min. Two hours later, two identical objects (A and

Please cite this article in press as: Zafra-Puerta et al., Gene therapy for Lafora disease in the *Epm2a*$^{-/-}$ mouse model, Molecular Therapy (2024), https://doi.org/10.1016/j.ymthe.2024.05.032

B) were placed in the center of the box. Each mouse had 10 min to freely explore the objects with exploration times (tA and tB) recorded. After 2 h, a new object (C) replaced object B, and the exploration times (tA and tC) were measured. Virtual timers generated by the XNote Stopwatch software were used to measure exploration times when mice examined objects from 2 cm or less. A discrimination index (DI) was calculated using the following equation: DI = (tC − tA)/(tC + tA).

Motor coordination

Motor coordination and balance were assessed using the rotarod test (Harvard Apparatus, Holliston, MA, USA). The mice underwent 2 days of training. On the first day, mice were placed on the rotarod at a constant speed of 4 rpm for 60 s. On the second day, they were trained with speed increasing from 4 to 8 rpm. Only mice able to stay on the rod for 60 s were included in the tests to minimize learning-related variations. In subsequent test sessions over 2 days, the latency time to fall from the cylinder was recorded during two sessions each day, with speed increasing from 4 to 40 rpm, and a maximum time limit of 5 min.

Spontaneous locomotor activity

Spontaneous movements were monitored with a computerized actimeter (Harvard Apparatus, Holliston, MA, USA) that recorded the number of times each mouse crossed the open field through infrared light beam breaks. The SEDACOM 1.4 software (Harvard Apparatus, Holliston, MA, USA) was utilized to analyze the spontaneous, rearing, and stereotyped movements at intervals of 5, 10, 15, 30, 45, and 60 min.

Video-EEG analysis

A plastic pedestal (Plastics1, Virginia, USA) with trimmed electrodes was surgically implanted and secured with acrylic resin onto the skull. Post-surgical pain was managed with meloxicam (5 mg/kg) (Boehringer Ingelheim, GA, USA). Animals were allowed 1 week for recovery before testing. Video-EEG recordings were obtained using a wireless transmitter (Epoch, CA, USA) attached to the pedestal, and the data were digitally recorded on a computer under free-motion conditions. Mice were observed in their home cages under basal conditions and, after 48 h, recorded for 30 min following PTZ injections. The sampling rate was 250 Hz and a 50-Hz notch filter was applied. Mouse behavior was captured using digital video cameras. EEG data were analyzed automatically and manually using the Acknowledge 5.0 software (Epoch, CA, USA) excluding periods with signal loss or artifacts. After applying the Comb Band Stop filter and a Blackman window, power spectra were calculated using a spectral estimator based on autoregressive processes ensuring normalized amplitudes for consistent peak-to-peak ranges. An automated seizure analysis was also conducted, closely monitoring and thoroughly analyzing both seizures and IEDs in the video-EEG recordings.

Sensitivity to PTZ

To analyze neuronal hyperexcitability, PTZ was administered via intraperitoneal injection, using two doses: 30 mg/kg (subconvulsive dose, rarely causing GTC seizures in WT animals) and 50 mg/kg (convulsive dose). The subconvulsive dose was used to determine the percentage of mice displaying myoclonic jerks. The convulsive dose was administered to evaluate the percentage of animals experiencing GTC seizures, their duration, the time to the first myoclonic or GTC seizure, and the lethality. Each animal was observed for 45 min by two researchers.

Electrophysiology

Mice were sacrificed by cervical dislocation. Brain collection and slice preparation were performed as previously reported.[83] For whole-cell patch-clamp recordings, pyramidal neurons of the CA1 and granule cells of the DG were visualized using infrared differential interference contrast (Olympus). Thin-wall borosilicate glass electrodes (3–6 MΩ) were filled with (in mM) K-gluconate 120, KCl 20, $MgCl_2$ 2, EGTA 0.02, HEPES 10, Mg-ATP 2, and Na-GTP 0.3 (pH 7.4). Access resistance was monitored online throughout each experiment and recordings were discarded if either access resistance or holding current increased by more than 25% during the experiment. No liquid junction potential correction was implemented. Membrane capacitance and resistance were taken online from the membrane seal test function of pClamp 10.7 (−5 mV step, 10 ms). Injection of depolarizing and hyperpolarizing current steps (1,200 ms, 50-pA increments) were used to obtain current-voltage curves and AP numbers at suprathreshold responses. Depolarizing current steps of increasing amplitudes (5-pA increments) were used to determine the AP threshold and rheobase currents. When recording spontaneous excitatory postsynaptic currents (sEPSCs), picrotoxin (50 ΩM) was added to the ACSF to block GABAA currents. Neurons were clamped at the holding potential (Vh) of −60 mV (CA1) and −70 mV (DG). Data were acquired with pClamp 10.7 (Molecular Devices) and currents were filtered at 0.1 kHz, digitized at 200 μs using Clampex 10.7, analyzed offline using the automatic detection, and subsequently checked manually for accuracy.

For extracellular recordings, the Axoclamp 2B amplifier (Molecular Devices, MA, USA) was used. The stimulating electrode was inserted into the Schaffer collaterals or in the perforant path fibers and the recording electrode, made of borosilicate glass capillaries filled with 2 M NaCl (resistance 10–15 MΩ), was placed into the stratum radiatum of the cornu ammonis 1 (CA1) or in the DG close to the granular layer, respectively. Epileptic-like activity in hippocampal DG was induced as previously reported.[42,83] LTP was induced by high-frequency stimulation (HFS) at 100 Hz (1 s), consisting of one train of stimuli for the CA1 area and three trains (5-min intervals) for the DG area, after recording a stable baseline for 10 min. Traces were filtered at 3 kHz, digitized at 10 kHz, and stored. The initial slope (for the CA1) and PS amplitude (for DG) of extracellular fEPSPs were used to assess alterations in synaptic strength.

Differential quantitative proteomics by isobaric labeling: TMT11plex

For differential quantitation in the proteomic and phosphoproteomic analysis, peptides were labeled with the tandem mass tag 11 plex

(TMT11-Plex) technique. Identification and quantification of proteins were performed using liquid chromatography coupled with tandem mass spectrometry (LC-MS/MS).[84,85]

Data were analyzed using a logarithmic statistical model (log2), enabling the estimation of peptide and protein abundances (Zq). For the identification of alterations in functional biological processes beyond individual protein responses, each category was assigned a category Z value (Zc). This facilitated the analysis of coordinated protein changes within categories. Finally, for the quantification of changes in peptide phosphorylation, the abundance of phospho-peptides was assessed using the corresponding standardized log2 ratio (Zp).[84,85]

Statistical analysis

Values are presented as means ± SEM or standard deviation (SD) or as percentages. To analyze the differences between experimental groups, we employed one- or two-way ANOVA, Fisher's exact test, Student's t test, and non-parametric Kruskal-Wallis or Mann-Whitney test, as indicated in each specific case. For EEG analysis, the area under the curve (AUC) was obtained to compare the differences in the power spectra between groups. For proteomics and phosphoproteomics, changes in protein abundance, categories, and abundance of phospho-peptides were determined by comparing the means of Zq, Zc, and Zp, respectively, between groups and selecting those with a p value of 0.05 or lower. For electrophysiological recordings, data analysis was performed offline using Clampfit 10.7 (Molecular Devices). Statistical analyses were conducted using GraphPad Prism 8.0 or GraphPad Prism 9.0 (GraphPad Software, San Diego, CA, USA). Statistical tests were two tailed and the statistical significance thresholds were denoted as $^{*}p < 0.05$, $^{**}p < 0.01$, $^{***}p < 0.001$, and $^{****}p < 0.0001$.

DATA AND CODE AVAILABILITY

Data supporting the findings of this study are available from the corresponding author.

SUPPLEMENTAL INFORMATION

Supplemental information can be found online at https://doi.org/10.1016/j.ymthe.2024.05.032.

ACKNOWLEDGMENTS

This work was supported by grants from the Spanish Ministry of Economy (Rti2018-095784b-100SAF MCI/AEI/FEDER, UE) to J.M.S. and M.P.S.; from the Tatiana Perez de Guzman el Bueno Foundation to M.P.S. and J.M.S.; from the Centro de Investigación Biomédica en Red de Enfermedades Raras (CIBERER) (ACCI 2020, 23 - U744) to M.P.S.; from the Fondazione Malattie Rare Mauro Baschirotto BIRD Onlus to M.P.S., C.C., M.S., and L.Z.P.; and a grant from the National Institute of Neurological Disorders and Stroke of the National Institutes of Health (P01NS097197), which established the Lafora Epilepsy Cure Initiative (LECI), to J.M.S. and M.P.S. We thank Pascual Sanz Bigorra (Institute of Biomedicine of Valencia [IBV]) and Manuel Soto Catalán (Instituto de Investigación Sanitaria-Fundación Jiménez Díaz) for their generous gift of GS, BiP, and cleaved caspase-3 antibodies, and to Miguel Chillón Rodríguez (Viral Vector Production Unit or UPV-UAB-VHIR) for the generation of rAAVs and technical advice. We also thank Juan Antonio López del Olmo (CNIC Proteomics Unit), Ariadna Martín Blázquez (Instituto de Investigación Sanitaria-Fundación Jiménez Díaz), and the Animal Facility of Instituto de Investigación Sanitaria-Fundación Jiménez Díaz for their technical assistance.

AUTHOR CONTRIBUTIONS

L.Z.-P., conceptualization, data curation, formal analysis, funding acquisition, investigation, methodology, validation, visualization, writing – original draft, and writing – review & editing; N.I.-C., conceptualization, data curation, investigation, and methodology; D.F.B., conceptualization, data curation, investigation, and methodology; M.S., data curation, formal analysis, funding acquisition, investigation, methodology, and writing – original draft; J.G.-F., conceptualization, investigation, and methodology; L.B., formal analysis and investigation; J.C., formal analysis and investigation; G.S.-M., data curation, formal analysis, and methodology; C.C., formal analysis, funding acquisition, investigation, supervision, validation, visualization, writing – original draft, and writing – review & editing; M.P.S., conceptualization, formal analysis, funding acquisition, investigation, project administration, supervision, validation, visualization, writing – original draft, and writing – review & editing; J.M.S., conceptualization, formal analysis, funding acquisition, investigation, project administration, supervision, validation, visualization, writing – original draft, and writing – review & editing.

DECLARATION OF INTERESTS

The authors report no competing interests.

REFERENCES

1. Lafora, G.R., and Glueck, B. (1911). Beitrag zur Histopathologie der myoklonischen Epilepsie. Z. F. D. G. Neur. U. Psych. *6*, 1–14. https://doi.org/10.1007/BF02863929.
2. Berkovic, S.F., Andermann, F., Carpenter, S., and Wolfe, L.S. (1986). Progressive myoclonus epilepsies: specific causes and diagnosis. EnglandN. Engl. J. Med. *315*, 296–305. https://doi.org/10.1056/nejm198607313150506.
3. Ham, M.W.V.H.T., and Jager, H.D. (1963). Progressive Myoclonus Epilepsy with Lafora Bodies. Clinical-Pathological Features. Epilepsia *4*, 95–119.
4. Turnbull, J., Tiberia, E., Striano, P., Genton, P., Carpenter, S., Ackerley, C.A., and Minassian, B.A. (2016). Lafora disease. Epileptic Disord. *18*, 38–62. https://doi.org/10.1684/epd.2016.0842.
5. Minassian, B.A., Lee, J.R., Herbrick, J.A., Huizenga, J., Soder, S., Mungall, A.J., Dunham, I., Gardner, R., Fong, C.Y., Carpenter, S., et al. (1998). Mutations in a gene encoding a novel protein tyrosine phosphatase cause progressive myoclonus epilepsy. Nat. Genet. *20*, 171–174. https://doi.org/10.1038/2470.
6. Serratosa, J.M., Gómez-Garre, P., Gallardo, M.E., Anta, B., de Bernabé, D.B., Lindhout, D., Augustijn, P.B., Tassinari, C.A., Malafosse, R.M., Topcu, M., et al. (1999). A novel protein tyrosine phosphatase gene is mutated in progressive myoclonus epilepsy of the Lafora type (EPM2). Hum. Mol. Genet. *8*, 345–352. https://doi.org/10.1093/hmg/8.2.345.
7. Ganesh, S., Agarwala, K.L., Ueda, K., Akagi, T., Shoda, K., Usui, T., Hashikawa, T., Osada, H., Delgado-Escueta, A.V., and Yamakawa, K. (2000). Laforin, defective in the progressive myoclonus epilepsy of Lafora type, is a dual-specificity phosphatase associated with polyribosomes. Hum. Mol. Genet. *9*, 2251–2261.

Please cite this article in press as: Zafra-Puerta et al., Gene therapy for Lafora disease in the *Epm2a*$^{-/-}$ mouse model, Molecular Therapy (2024), https://doi.org/10.1016/j.ymthe.2024.05.032

8. Serratosa, J.M., Delgado-Escueta, A.V., Posada, I., Shih, S., Drury, I., Berciano, J., Zabala, J.A., Antúnez, M.C., and Sparkes, R.S. (1995). The gene for progressive myoclonus epilepsy of the Lafora type maps to chromosome 6q. Hum. Mol. Genet. *4*, 1657–1663. https://doi.org/10.1093/hmg/4.9.1657.

9. Chan, E.M., Young, E.J., Ianzano, L., Munteanu, I., Zhao, X., Christopoulos, C.C., Avanzini, G., Elia, M., Ackerley, C.A., Jovic, N.J., et al. (2003). Mutations in NHLRC1 cause progressive myoclonus epilepsy. Nat. Genet. *35*, 125–127. https://doi.org/10.1038/ng1238.

10. Gentry, M.S., Worby, C.A., and Dixon, J.E. (2005). Insights into Lafora disease: malin is an E3 ubiquitin ligase that ubiquitinates and promotes the degradation of laforin. Proc. Natl. Acad. Sci. USA *102*, 8501–8506. https://doi.org/10.1073/pnas.0503285102.

11. Gentry, M.S., Romá-Mateo, C., and Sanz, P. (2013). Laforin, a protein with many faces: glucan phosphatase, adapter protein, et alii. FEBS J. *280*, 525–537. https://doi.org/10.1111/j.1742-4658.2012.08549.x.

12. Vilchez, D., Ros, S., Cifuentes, D., Pujadas, L., Vallès, J., García-Fojeda, B., Criado-García, O., Fernández-Sánchez, E., Medraño-Fernández, I., Domínguez, J., et al. (2007). Mechanism suppressing glycogen synthesis in neurons and its demise in progressive myoclonus epilepsy. Nat. Neurosci. *10*, 1407–1413. https://doi.org/10.1038/nn1998.

13. Garyali, P., Siwach, P., Singh, P.K., Puri, R., Mittal, S., Sengupta, S., Parihar, R., and Ganesh, S. (2009). The malin-laforin complex suppresses the cellular toxicity of misfolded proteins by promoting their degradation through the ubiquitin-proteasome system. Hum. Mol. Genet. *18*, 688–700. https://doi.org/10.1093/hmg/ddn398.

14. Lafora, G.R. (1911). Über das Vorkommen amyloider Körperchen im Innern der Ganglienzellen. Virchows Arch. Path. Anat. *205*, 295–303. https://doi.org/10.1007/BF01989438.

15. Yokoi, S., Austin, J., Witmer, F., and Sakai, M. (1968). Studies in myoclonus epilepsy (Lafora body form). I. Isolation and preliminary characterization of Lafora bodies in two cases. Arch. Neurol. *19*, 15–33. https://doi.org/10.1001/archneur.1968.00480010033002.

16. Sullivan, M.A., Nitschke, S., Steup, M., Minassian, B.A., and Nitschke, F. (2017). Pathogenesis of Lafora Disease: Transition of Soluble Glycogen to Insoluble Polyglucosan. Int. J. Mol. Sci. *18*, 1743.

17. Gentry, M.S., Guinovart, J.J., Minassian, B.A., Roach, P.J., and Serratosa, J.M. (2018). Lafora disease offers a unique window into neuronal glycogen metabolism. J. Biol. Chem. *293*, 7117–7125. https://doi.org/10.1074/jbc.R117.803064.

18. Romá-Mateo, C., Aguado, C., García-Giménez, J.L., Knecht, E., Sanz, P., and Pallardó, F.V. (2015). Oxidative stress, a new hallmark in the pathophysiology of Lafora progressive myoclonus epilepsy. Free Radic. Biol. Med. *88*, 30–41. https://doi.org/10.1016/j.freeradbiomed.2015.01.034.

19. Vernia, S., Rubio, T., Heredia, M., Rodríguez de Córdoba, S., and Sanz, P. (2009). Increased endoplasmic reticulum stress and decreased proteasomal function in lafora disease models lacking the phosphatase laforin. PloS one *4*, e5907. https://doi.org/10.1371/journal.pone.0005907.

20. Liu, Y., Wang, Y., Wu, C., Liu, Y., and Zheng, P. (2009). Deletions and missense mutations of EPM2A exacerbate unfolded protein response and apoptosis of neuronal cells induced by endoplasm reticulum stress. Hum. Mol. Genet. *18*, 2622–2631. https://doi.org/10.1093/hmg/ddp196.

21. Ganesh, S., Delgado-Escueta, A.V., Sakamoto, T., Avila, M.R., Machado-Salas, J., Hoshii, Y., Akagi, T., Gomi, H., Suzuki, T., Amano, K., et al. (2002). Targeted disruption of the Epm2a gene causes formation of Lafora inclusion bodies, neurodegeneration, ataxia, myoclonus epilepsy and impaired behavioral response in mice. Hum. Mol. Genet. *11*, 1251–1262. https://doi.org/10.1093/hmg/11.11.1251.

22. Criado, O., Aguado, C., Gayarre, J., Duran-Trio, L., Garcia-Cabrero, A.M., Vernia, S., San Millán, B., Heredia, M., Romá-Mateo, C., Mouron, S., et al. (2012). Lafora bodies and neurological defects in malin-deficient mice correlate with impaired autophagy. Hum. Mol. Genet. *21*, 1521–1533. https://doi.org/10.1093/hmg/ddr590.

23. García-Cabrero, A.M., Marinas, A., Guerrero, R., de Córdoba, S.R., Serratosa, J.M., and Sánchez, M.P. (2012). Laforin and malin deletions in mice produce similar neurologic impairments. J. Neuropathol. Exp. Neurol. *71*, 413–421. https://doi.org/10.1097/NEN.0b013e318253350f.

24. Burgos, D.F., Machío-Castello, M., Iglesias-Cabeza, N., Giráldez, B.G., González-Fernández, J., Sánchez-Martín, G., Sánchez, M.P., and Serratosa, J.M. (2023). Early Treatment with Metformin Improves Neurological Outcomes in Lafora Disease. Neurotherapeutics *20*, 230–244. https://doi.org/10.1007/s13311-022-01304-w.

25. Berthier, A., Payá, M., García-Cabrero, A.M., Ballester, M.I., Heredia, M., Serratosa, J.M., Sánchez, M.P., and Sanz, P. (2016). Pharmacological Interventions to Ameliorate Neuropathological Symptoms in a Mouse Model of Lafora Disease. Mol. Neurobiol. *53*, 1296–1309. https://doi.org/10.1007/s12035-015-9091-8.

26. Bisulli, F., Muccioli, L., d'Orsi, G., Canafoglia, L., Freri, E., Licchetta, L., Mostacci, B., Riguzzi, P., Pondrelli, F., Avolio, C., et al. (2019). Treatment with metformin in twelve patients with Lafora disease. Orphanet J. Rare Dis. *14*, 149. https://doi.org/10.1186/s13023-019-1132-3.

27. Sánchez-Elexpuru, G., Serratosa, J.M., and Sánchez, M.P. (2017). Sodium selenate treatment improves symptoms and seizure susceptibility in a malin-deficient mouse model of Lafora disease. Epilepsia *58*, 467–475. https://doi.org/10.1111/epi.13656.

28. Brewer, M.K., Uittenbogaard, A., Austin, G.L., Segvich, D.M., DePaoli-Roach, A., Roach, P.J., McCarthy, J.J., Simmons, Z.R., Brandon, J.A., Zhou, Z., et al. (2019). Targeting Pathogenic Lafora Bodies in Lafora Disease Using an Antibody-Enzyme Fusion. Cell Metab. *30*, 689–705.e6. https://doi.org/10.1016/j.cmet.2019.07.002.

29. Ahonen, S., Nitschke, S., Grossman, T.R., Kordasiewicz, H., Wang, P., Zhao, X., Guisso, D.R., Kasiri, S., Nitschke, F., and Minassian, B.A. (2021). Gys1 antisense therapy rescues neuropathological bases of murine Lafora disease. Brain. *144*, 2985–2993. https://doi.org/10.1093/brain/awab194.

30. Mollá, B., Heredia, M., and Sanz, P. (2021). Modulators of Neuroinflammation Have a Beneficial Effect in a Lafora Disease Mouse Model. Mol. Neurobiol. *58*, 2508–2522. https://doi.org/10.1007/s12035-021-02285-1.

31. Gumusgoz, E., Guisso, D.R., Kasiri, S., Wu, J., Dear, M., Verhalen, B., Nitschke, S., Mitra, S., Nitschke, F., and Minassian, B.A. (2021). Targeting Gys1 with AAV-SaCas9 Decreases Pathogenic Polyglucosan Bodies and Neuroinflammation in Adult Polyglucosan Body and Lafora Disease Mouse Models. Neurotherapeutics *18*, 1414–1425. https://doi.org/10.1007/s13311-021-01040-7.

32. Gumusgoz, E., Kasiri, S., Guisso, D.R., Wu, J., Dear, M., Verhalen, B., and Minassian, B.A. (2022). AAV-Mediated Artificial miRNA Reduces Pathogenic Polyglucosan Bodies and Neuroinflammation in Adult Polyglucosan Body and Lafora Disease Mouse Models. Neurotherapeutics *19*, 982–993. https://doi.org/10.1007/s13311-022-01218-7.

33. Merten, O.W., Gény-Fiamma, C., and Douar, A.M. (2005). Current issues in adeno-associated viral vector production. Gene Ther. *12*, S51–S61. https://doi.org/10.1038/sj.gt.3302615.

34. Wu, Z., Asokan, A., and Samulski, R.J. (2006). Adeno-associated virus serotypes: vector toolkit for human gene therapy. Mol. Ther. *14*, 316–327.

35. Li, C., and Samulski, R.J. (2020). Engineering adeno-associated virus vectors for gene therapy. Nat. Rev. Genet. *21*, 255–272. https://doi.org/10.1038/s41576-019-0205-4.

36. Hastie, E., and Samulski, R.J. (2015). Adeno-associated virus at 50: a golden anniversary of discovery, research, and gene therapy success–a personal perspective. Hum. Gene Ther. *26*, 257–265.

37. Chan, K.Y., Jang, M.J., Yoo, B.B., Greenbaum, A., Ravi, N., Wu, W.L., Sánchez-Guardado, L., Lois, C., Mazmanian, S.K., Deverman, B.E., and Gradinaru, V. (2017). Engineered AAVs for efficient noninvasive gene delivery to the central and peripheral nervous systems. Nat. Neurosci. *20*, 1172–1179. https://doi.org/10.1038/nn.4593.

38. He, X., Xie, H., Liu, X., and Gu, F. (2019). Basic and Clinical Application of Adeno-Associated Virus-Mediated Genome Editing. Hum. Gene Ther. *30*, 673–681.

39. Hudry, E., Andres-Mateos, E., Lerner, E.P., Volak, A., Cohen, O., Hyman, B.T., Maguire, C.A., and Vandenberghe, L.H. (2018). Efficient Gene Transfer to the Central Nervous System by Single-Stranded Anc80L65. Mol. Ther. Methods Clin. Dev. *10*, 197–209. https://doi.org/10.1016/j.omtm.2018.07.006.

40. Marcó, S., Haurigot, V., Jaén, M.L., Ribera, A., Sánchez, V., Molas, M., Garcia, M., León, X., Roca, C., Sánchez, X., et al. (2021). Seven-year follow-up of durability and safety of AAV CNS gene therapy for a lysosomal storage disorder in a large animal. Mol. Ther. Methods Clin. Dev. *23*, 370–389. https://doi.org/10.1016/j.omtm.2021.09.017.

41. Cearley, C.N., and Wolfe, J.H. (2006). Transduction characteristics of adeno-associated virus vectors expressing cap serotypes 7, 8, 9, and Rh10 in the mouse brain. Mol. Ther. *13*, 528–537. https://doi.org/10.1016/j.ymthe.2005.11.015.

42. Costa, C., Parnetti, L., D'Amelio, M., Tozzi, A., Tantucci, M., Romigi, A., Siliquini, S., Cavallucci, V., Di Filippo, M., Mazzocchetti, P., et al. (2016). Epilepsy, amyloid-β, and D1 dopamine receptors: a possible pathogenetic link? Neurobiol. Aging *48*, 161–171. https://doi.org/10.1016/j.neurobiolaging.2016.08.025.

43. Rao, S.N.R., Maity, R., Sharma, J., Dey, P., Shankar, S.K., Satishchandra, P., and Jana, N.R. (2010). Sequestration of chaperones and proteasome into Lafora bodies and proteasomal dysfunction induced by Lafora disease-associated mutations of malin. Hum. Mol. Genet. *19*, 4726–4734. https://doi.org/10.1093/hmg/ddq407.

44. Sinadinos, C., Valles-Ortega, J., Boulan, L., Solsona, E., Tevy, M.F., Marquez, M., Duran, J., Lopez-Iglesias, C., Calbó, J., Blasco, E., et al. (2014). Neuronal glycogen synthesis contributes to physiological aging. Aging cell *13*, 935–945. https://doi.org/10.1111/acel.12254.

45. Lohi, H., Ianzano, L., Zhao, X.C., Chan, E.M., Turnbull, J., Scherer, S.W., Ackerley, C.A., and Minassian, B.A. (2005). Novel glycogen synthase kinase 3 and ubiquitination pathways in progressive myoclonus epilepsy. Hum. Mol. Genet. *14*, 2727–2736. https://doi.org/10.1093/hmg/ddi306.

46. Mittal, S., Dubey, D., Yamakawa, K., and Ganesh, S. (2007). Lafora disease proteins malin and laforin are recruited to aggresomes in response to proteasomal impairment. Hum. Mol. Genet. *16*, 753–762. https://doi.org/10.1093/hmg/ddm006.

47. Aguado, C., Sarkar, S., Korolchuk, V.I., Criado, O., Vernia, S., Boya, P., Sanz, P., de Córdoba, S.R., Knecht, E., and Rubinsztein, D.C. (2010). Laforin, the most common protein mutated in Lafora disease, regulates autophagy. Hum. Mol. Genet. *19*, 2867–2876. https://doi.org/10.1093/hmg/ddq190.

48. Knecht, E., Aguado, C., Sarkar, S., Korolchuk, V.I., Criado-García, O., Vernia, S., Boya, P., Sanz, P., Rodríguez de Córdoba, S., and Rubinsztein, D.C. (2010). Impaired autophagy in Lafora disease. Autophagy *6*, 991–993. https://doi.org/10.4161/auto6.7.13308.

49. Lahuerta, M., Aguado, C., Sánchez-Martín, P., Sanz, P., and Knecht, E. (2018). Degradation of altered mitochondria by autophagy is impaired in Lafora disease. FEBS J. *285*, 2071–2090. https://doi.org/10.1111/febs.14468.

50. Romá-Mateo, C., Aguado, C., García-Giménez, J.L., Ibáñez-Cabellos, J.S., Seco-Cervera, M., Pallardó, F.V., Knecht, E., and Sanz, P. (2015). Increased oxidative stress and impaired antioxidant response in Lafora disease. Mol. Neurobiol. *51*, 932–946. https://doi.org/10.1007/s12035-014-8747-0.

51. Upadhyay, M., Agarwal, S., Bhadauriya, P., and Ganesh, S. (2017). Loss of laforin or malin results in increased Drp1 level and concomitant mitochondrial fragmentation in Lafora disease mouse models. Neurobiol. Dis. *100*, 39–51. https://doi.org/10.1016/j.nbd.2017.01.002.

52. Muñoz-Ballester, C., Berthier, A., Viana, R., and Sanz, P. (2016). Homeostasis of the astrocytic glutamate transporter GLT-1 is altered in mouse models of Lafora disease. Biochim. Biophys. Acta *1862*, 1074–1083. https://doi.org/10.1016/j.bbadis.2016.03.008.

53. Muñoz-Ballester, C., Santana, N., Perez-Jimenez, E., Viana, R., Artigas, F., and Sanz, P. (2019). In vivo glutamate clearance defects in a mouse model of Lafora disease. Exp. Neurol. *320*, 112959. https://doi.org/10.1016/j.expneurol.2019.112959.

54. Perez-Jimenez, E., Viana, R., Muñoz-Ballester, C., Vendrell-Tornero, C., Moll-Diaz, R., Garcia-Gimeno, M.A., and Sanz, P. (2021). Endocytosis of the glutamate transporter 1 is regulated by laforin and malin: Implications in Lafora disease. Glia *69*, 1170–1183. https://doi.org/10.1002/glia.23956.

55. Duran, J., Gruart, A., García-Rocha, M., Delgado-García, J.M., and Guinovart, J.J. (2014). Glycogen accumulation underlies neurodegeneration and autophagy impairment in Lafora disease. Hum. Mol. Genet. *23*, 3147–3156. https://doi.org/10.1093/hmg/ddu024.

56. Duran, J., Hervera, A., Markussen, K.H., Varea, O., López-Soldado, I., Sun, R.C., Del Río, J.A., Gentry, M.S., and Guinovart, J.J. (2021). Astrocytic glycogen accumulation drives the pathophysiology of neurodegeneration in Lafora disease. Brain. *144*, 2349–2360. https://doi.org/10.1093/brain/awab110.

57. López-González, I., Viana, R., Sanz, P., and Ferrer, I. (2017). Inflammation in Lafora Disease: Evolution with Disease Progression in Laforin and Malin Knock-out Mouse Models. Mol. Neurobiol. *54*, 3119–3130. https://doi.org/10.1007/s12035-016-9884-4.

58. Romá-Mateo, C., Lorente-Pozo, S., Márquez-Thibaut, L., Moreno-Estellés, M., Garcés, C., González, D., Lahuerta, M., Aguado, C., García-Giménez, J.L., Sanz, P., et al. (2023). Age-Related microRNA Overexpression in Lafora Disease Male Mice Provides Links between Neuroinflammation and Oxidative Stress. Int. J. Mol. Sci. *24*, 1089. https://doi.org/10.3390/ijms24021089.

59. Lahuerta, M., Gonzalez, D., Aguado, C., Fathinajafabadi, A., García-Giménez, J.L., Moreno-Estellés, M., Romá-Mateo, C., Knecht, E., Pallardó, F.V., and Sanz, P. (2020). Reactive Glia-Derived Neuroinflammation: a Novel Hallmark in Lafora Progressive Myoclonus Epilepsy That Progresses with Age. Mol. Neurobiol. *57*, 1607–1621. https://doi.org/10.1007/s12035-019-01842-z.

60. Sánchez-Elexpuru, G., Serratosa, J.M., Sanz, P., and Sánchez, M.P. (2017). 4-Phenylbutyric acid and metformin decrease sensitivity to pentylenetetrazol-induced seizures in a malin knockout model of Lafora disease. Neuroreport *28*, 268–271. https://doi.org/10.1097/wnr.0000000000000751.

61. Sinha, P., Verma, B., and Ganesh, S. (2021). Trehalose Ameliorates Seizure Susceptibility in Lafora Disease Mouse Models by Suppressing Neuroinflammation and Endoplasmic Reticulum Stress. Mol. Neurobiol. *58*, 1088–1101. https://doi.org/10.1007/s12035-020-02170-3.

62. García-Giménez, J.L., Seco-Cervera, M., Aguado, C., Romá-Mateo, C., Dasí, F., Priego, S., Markovic, J., Knecht, E., Sanz, P., and Pallardó, F.V. (2013). Lafora disease fibroblasts exemplify the molecular interdependence between thioredoxin 1 and the proteasome in mammalian cells. Free Radic. Biol. Med. *65*, 347–359. https://doi.org/10.1016/j.freeradbiomed.2013.07.001.

63. Zhang, Y., He, X., Meng, X., Wu, X., Tong, H., Zhang, X., and Qu, S. (2017). Regulation of glutamate transporter trafficking by Nedd4-2 in a Parkinson's disease model. Cell Death Dis. *8*, e2574. https://doi.org/10.1038/cddis.2016.454.

64. Medvedev, A., Mackenzie, L., Hiscock, J.J., and Willoughby, J.O. (2000). Kainic acid induces distinct types of epileptiform discharge with differential involvement of hippocampus and neocortex. Brain Res. Bull. *52*, 89–98. https://doi.org/10.1016/s0361-9230(00)00239-2.

65. Medvedev, A., and Willoughby, J.O. (1999). Autoregressive modeling of the EEG in systemic kainic acid-induced epileptogenesis. Int. J. Neurosci. *97*, 149–167. https://doi.org/10.3109/00207459909000657.

66. Willoughby, J.O., Fitzgibbon, S.P., Pope, K.J., Mackenzie, L., Medvedev, A.V., Clark, C.R., Davey, M.P., and Wilcox, R.A. (2003). Persistent abnormality detected in the non-ictal electroencephalogram in primary generalised epilepsy. J. Neurol. Neurosurg. Psychiatry *74*, 51–55. https://doi.org/10.1136/jnnp.74.1.51.

67. Marrosu, F., Santoni, F., Fà, M., Puligheddu, M., Barberini, L., Genugu, F., Frau, R., Manunta, M., and Mereu, G. (2006). Beta and gamma range EEG power-spectrum correlation with spiking discharges in DBA/2J mice absence model: role of GABA receptors. Epilepsia *47*, 489–494. https://doi.org/10.1111/j.1528-1167.2006.00456.x.

68. Spoleti, E., Krashia, P., La Barbera, L., Nobili, A., Lupascu, C.A., Giacalone, E., Keller, F., Migliore, M., Renzi, M., and D'Amelio, M. (2022). Early derailment of firing properties in CA1 pyramidal cells of the ventral hippocampus in an Alzheimer's disease mouse model. Exp. Neurol. *350*, 113969. https://doi.org/10.1016/j.expneurol.2021.113969.

69. Girardeau, G., and Lopes-Dos-Santos, V. (2021). Brain neural patterns and the memory function of sleep. Science (New York, N.Y.) *374*, 560–564. https://doi.org/10.1126/science.abi8370.

70. Meier, K., Merseburg, A., Isbrandt, D., Marguet, S.L., and Morellini, F. (2020). Dentate Gyrus Sharp Waves, a Local Field Potential Correlate of Learning in the Dentate Gyrus of Mice. J. Neurosci. *40*, 7105–7118. https://doi.org/10.1523/jneurosci.2275-19.2020.

Please cite this article in press as: Zafra-Puerta et al., Gene therapy for Lafora disease in the *Epm2a*$^{-/-}$ mouse model, Molecular Therapy (2024), https://doi.org/10.1016/j.ymthe.2024.05.032

71. Kullmann, D.M., Asztely, F., and Walker, M.C. (2000). The role of mammalian ionotropic receptors in synaptic plasticity: LTP, LTD and epilepsy. Cell. Mol. Life Sci. *57*, 1551–1561. https://doi.org/10.1007/pl00000640.

72. During, M.J., Ryder, K.M., and Spencer, D.D. (1995). Hippocampal GABA transporter function in temporal-lobe epilepsy. Nature *376*, 174–177. https://doi.org/10.1038/376174a0.

73. Chawla, A.R., Johnson, D.E., Zybura, A.S., Leeds, B.P., Nelson, R.M., and Hudmon, A. (2017). Constitutive regulation of the glutamate/aspartate transporter EAAT1 by Calcium-Calmodulin-Dependent Protein Kinase II. J. Neurochem. *140*, 421–434. https://doi.org/10.1111/jnc.13913.

74. Mahmoud, S., Gharagozloo, M., Simard, C., and Gris, D. (2019). Astrocytes Maintain Glutamate Homeostasis in the CNS by Controlling the Balance between Glutamate Uptake and Release. Cells *8*, 184.

75. Héja, L., Nyitrai, G., Kékesi, O., Dobolyi, A., Szabó, P., Fiáth, R., Ulbert, I., Pál-Szenthe, B., Palkovits, M., and Kardos, J. (2012). Astrocytes convert network excitation to tonic inhibition of neurons. BMC Biol. *10*, 26. https://doi.org/10.1186/1741-7007-10-26.

76. Schroeder, B.C., Kubisch, C., Stein, V., and Jentsch, T.J. (1998). Moderate loss of function of cyclic-AMP-modulated KCNQ2/KCNQ3 K+ channels causes epilepsy. Nature *396*, 687–690. https://doi.org/10.1038/25367.

77. Park, K.S., Yang, J.W., Seikel, E., and Trimmer, J.S. (2008). Potassium channel phosphorylation in excitable cells: providing dynamic functional variability to a diverse family of ion channels. Physiol. (Bethesda, Md.) *23*, 49–57. https://doi.org/10.1152/physiol.00031.2007.

78. Ostendorf, A.P., and Wong, M. (2015). mTOR inhibition in epilepsy: rationale and clinical perspectives. CNS drugs *29*, 91–99. https://doi.org/10.1007/s40263-014-0223-x.

79. Citraro, R., Leo, A., Constanti, A., Russo, E., and De Sarro, G. (2016). mTOR pathway inhibition as a new therapeutic strategy in epilepsy and epileptogenesis. Pharmacol. Res. *107*, 333–343. https://doi.org/10.1016/j.phrs.2016.03.039.

80. Rubio, T., Viana, R., Moreno-Estellés, M., Campos-Rodríguez, Á., and Sanz, P. (2023). TNF and IL6/Jak2 signaling pathways are the main contributors of the glia-derived neuroinflammation present in Lafora disease, a fatal form of progressive myoclonus epilepsy. Neurobiol. Dis. *176*, 105964. https://doi.org/10.1016/j.nbd.2022.105964.

81. Pondrelli, F., Muccioli, L., Licchetta, L., Mostacci, B., Zenesini, C., Tinuper, P., Vignatelli, L., and Bisulli, F. (2021). Natural history of Lafora disease: a prognostic systematic review and individual participant data meta-analysis. Orphanet J. Rare Dis. *16*, 362. https://doi.org/10.1186/s13023-021-01989-w.

82. Piedra, J., Ontiveros, M., Miravet, S., Penalva, C., Monfar, M., and Chillon, M. (2015). Development of a rapid, robust, and universal picogreen-based method to titer adeno-associated vectors. Hum. Gene Ther. Methods *26*, 35–42.

83. Burgos, D.F., Sciaccaluga, M., Worby, C.A., Zafra-Puerta, L., Iglesias-Cabeza, N., Sánchez-Martín, G., Prontera, P., Costa, C., Serratosa, J.M., and Sánchez, M.P. (2023). Epm2a(R240X) knock-in mice present earlier cognitive decline and more epileptic activity than Epm2a(-/-) mice. Neurobiol. Dis. *181*, 106119. https://doi.org/10.1016/j.nbd.2023.106119.

84. Yuste-Montalvo, A., Fernandez-Bravo, S., Oliva, T., Pastor-Vargas, C., Betancor, D., Goikoetxea, M.J., Laguna, J.J., López, J.A., Alvarez-Llamas, G., Cuesta-Herranz, J., et al. (2021). Proteomic and Biological Analysis of an *In Vitro* Human Endothelial System in Response to Drug Anaphylaxis. Front. Immunol. *12*, 692569. https://doi.org/10.3389/fimmu.2021.692569.

85. Santiago-Hernandez, A., Martin-Lorenzo, M., Martínez, P.J., Gómez-Serrano, M., Lopez, J.A., Cannata, P., Esteban, V., Heredero, A., Aldamiz-Echevarria, G., Vázquez, J., et al. (2021). Early renal and vascular damage within the normoalbuminuria condition. J. Hypertens. *39*, 2220–2231. https://doi.org/10.1097/hjh.0000000000002936.